Article

Evaluating Halogen-Bond Strength as a Function of Molecular Structure Using Nuclear Magnetic Resonance Spectroscopy and Computational Analysis

Quang Minh Dang, Jeffrey H. Simpson, Carol A. Parish, and Michael C. Leopold*

Read Online
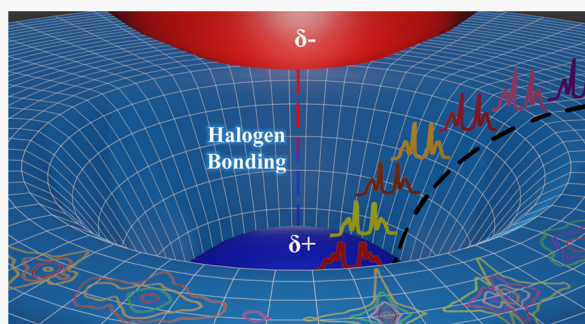
ACCESS | Metrics & More | Article Recommendations | Supporting Information

ABSTRACT: Halogen bonding (XB) is a highly directional, non-covalent intermolecular interaction between a molecule (XB donor) presenting a halogen with an electron-deficient region or sigma hole (σ-hole) and an electron-rich or Lewis-base molecule (XB acceptor). A systematic, experimental, and theoretical study of solution-phase XB strength as a function of the molecular structure for both XB donor and acceptor molecules is presented. The impact of specific structural features is assessed using ^{19}F and ^1H nuclear magnetic resonance (NMR) titrations to determine association constants, density functional theory calculations for interaction energies and bond lengths, as well as $^{19}F-^1H$ HOESY NMR measurements of intermolecular cross-relaxation between the interacting XB donor–acceptor adducts. For XB donor molecules (perfluoro-halogenated benzenes), results indicate the critical importance of iodine coupled with electron-withdrawing entities. Prominent structural components of XB acceptor molecules include a central atom working in conjunction with a Lewis-base atom to present high electron density directed at the σ-hole (e.g., tributylphosphine oxide). Additionally, larger surrounding aliphatic R groups (e.g., butyl and octyl) were found to significantly stabilize strong XB, particularly in solvents that promote the interaction. With a more thorough understanding of structure-optimized XB, one can envision harnessing XB interactions more strategically for specific design of optimal materials and chemical applications.
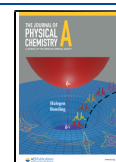
1. INTRODUCTION

The importance of intermolecular interactions is well-known throughout chemistry, biology, and materials science—small forces that can have a major impact on the properties of materials. While hydrogen bonding (HB), electrostatic interactions, and dispersion forces have been studied for over a century, the past two decades have seen increasing interests in the study and applications of halogen bonding (XB) interactions.[1,2] Despite this focus in recent decades, the scientific literature dedicated to investigating XB is still dwarfed by that of the more well-established, traditional intermolecular forces.[3] The XB studies that have appeared in the literature, however, make the case that XB is a highly relevant phenomenon in the chemistry of crystal engineering,[4,5] biology,[6–9] chromatography,[10,11] and materials science.[7] Additionally, there is growing evidence that XB can be used to detect anionic species in aqueous solutions[12–16] and to play a role in sensors targeting explosive molecules.[14,17] While the literature is replete with important applications of XB bonding, an experimentally based, fundamental study of the relationship between the molecular structure and XB interaction strength is necessary before the potential of XB bonding can be fully realized.

XB is a highly directional, non-covalent, and electrostatic interaction between a region of positive electrostatic potential on a halogen atom (XB donor) and a Lewis base (XB acceptor).[1,18] The region of positive electrostatic potential emerges as a result of the polarizability of a halogen atom bonded to electron (e^-) withdrawing entities that pull e^- density from the halogen atom along the σ bond axis. Such combination of factors creates a positively charged area ($\delta+$) known as a "sigma (σ) hole".[1,19,20] XB is more directionally constrained than HB due to the position of the σ-hole, which forms along the covalent bond of the halogen atom with another atom.[19,20] It is this linearity of the XB interactions that enables its employment in crystal engineering as well as with electrochemical detection of anions.[12–15,21,22] The σ-hole is highly tunable in that its size can be directly attributable to the specific halogen's polarizability and electronegativity as well as

9377

the strength of nearby e⁻-withdrawing groups (EWGs).[19,20] Larger σ-holes correlate to more effective XB donor capability and subsequent stronger XB interactions with XB acceptors. The strength of the XB interaction has been shown to be significant in specific cases including instances where it is preferred over HB interactions in crystal structures and in solution.[23−27] Shirman et al. used XB interactions to drive non-covalent assembly of gold NPs at planar surfaces[28] —film assembly previously achieved with more formidable inter-actions such as electrostatic linkages,[29] covalent ester coupling,[30] and/or HB interactions.[31] Taken collectively, these results indicate that XB can be a significant interaction that can be harnessed under specialized conditions.

A significant portion of the XB research found in the literature are fundamental theoretical/computational stud-ies,[32−39] whereas another fraction combines experimental work with complementary computational measure-ments.[17,40−43] Experimental evidence of XB often comes from examining the interaction in the vapor phase,[14,17] in the solid phase via X-ray crystallography,[27,44−46] or without considering the influence of solvent as in many theoretical investigations.[32−39] Experimental studies of XB in solution are significantly fewer in number. Hawthorne and co-workers in 2013 utilized Fourier transform infrared (FT-IR) spectroscopy to characterize changes in vibrational frequencies of hepta-fluoroiodopropane compounds (XB donors) and pyridine (XB acceptor) as a result of XB interactions.[47] In a 2011 study by Shen and Jin, XB interactions of 1,2-diiodoperfluoroethane and 1,6-diiodoperfluorohexane (XB donors) with several halide anions (XB acceptors) gave rise to distinct electronic transitions detected by UV−vis.[48] FT-IR and UV−vis measurements of XB interactions indicate the presence of XB adducts in solution or show only a semi-quantitative assessment of XB interaction strength.[2] Some solution measurements of XB make use of nuclear magnetic resonance (NMR) spectroscopy to measure the association constants (K_a) between the two interacting molecules that form an adduct—a widely accepted technique for assessing the strength of intermolecular interactions,[2,49] with very instructive reviews, tutorials, and online resources available (www.supramolecular. com).[12,21,40−42,49−51] Within these studies, however, there is no systematic examination of the structural properties of both the XB donor and the XB acceptor that impact the strength of XB interactions.

Prior gas-phase experimental and computational studies from our group[17] identified halogen-substituted arenes (e.g., dihalobenzenes and dihalotetrafluorobenzenes) as effective XB donors. Other reports have examined similarly structured aromatic XB donors as a component of their studies.[27,40,52] A highly formative report by Sarwar et al. in 2010 provided a combined theoretical and experimental examination of the structural and solvent effects on XB in solution—focusing on fluorinated iodoalkanes and iodoarenes and using ¹⁹F NMR to determine K_a values for adducts.[40] Sarwar and co-workers focused on the effects of substitutions *para* to iodine in perfluoroarene XB donors, solvent choices (discussed in Section 3.3 below), and structures of perfluoro-aromatic *versus* aliphatic donors on XB interactions. Results suggested that XB donors with e⁻-donating oxygen and nitrogen substituents—such as methoxy and piperidine groups, respectively—or milder e⁻-withdrawing substituents—such as phenyl—*para* to iodine exhibit less pronounced σ-holes and weaker XB interactions (lower K_a values) than iodopentafluorobenzene

(IPFB). The strongest XB interactions ($K_a = 34 \pm 7$ M⁻¹) were actually observed between a longer perfluorinated aliphatic XB donor ($C_8F_{17}I$) and a strong XB acceptor (quinuclidine). However, straight-chain XB donors typically offer less versatility for structural manipulation whereas aromatic donors can be modified in numerous ways with substitution at all five substituent positions on the ring. Despite not addressing the non-specific interactions evident from the titration curves, the well-done study of the Taylor group[40] represents an excellent starting point for a more systematic structural investigation conducted herein.

Other significant reports on XB interactions include studies done by the laboratories of Ciancaleoni[53] and Philp.[51] In brief, Ciancaleoni and co-workers used NMR spectroscopy to distinguish XB interactions from non-specific interactions between fluorinated aromatic as well as aliphatic XB donors (Br and I-substituted) with strong XB acceptors such as 1,4-diazabicyclooctane (DABCO) and 2,4,6-trimethylpyridine (Me₃Py). Their results show that the ratio of XB to non-specific interactions between different XB donors and accept-ors vary depending on the halogen atom of the XB donors and the strength of the XB acceptors. For example, the study showed that non-specific interactions were high (44%) between bromopentafluorobenzene and DABCO and low (4% or XB-dominated) in IPFB and DABCO adducts, emphasizing the important choice of the halogen atom in the formation of the σ-hole.[53] In another study, Maugeri et al. used ¹⁹F and ¹⁵N NMR spectroscopy to examine XB interactions using XB donors iodotriazoles *versus* IPFB and a small number of pyridine-based XB acceptors.[51] Of note, similar XB interactions were achieved for 1,4-diaryl-5-iodo-1,2,3-triazole ($K_a = 1.67$ M⁻¹) and IPFB (2.67 M⁻¹) (XB donors) with *para*-substituted pyridine XB acceptors. Beweries et al.[41] examined XB interactions between group 10 metal pincer compounds with IPFB and 1,4-diiodotetrafluoroben-zene whereas Otte et al.[52] performed a study showing significant nitrogen-to-iodine XB interactions over a distance of 2.9+ Å between iodobenzene (lacking EWGs on the aromatic ring) and quinuclidine. Quality XB studies of specific systems as in these reports are scattered throughout the literature and have formed the evidentiary foundation for our XB knowledge thus far.

In this study, a systematic evaluation of how structural parameters of both the XB donor and acceptor molecules affect XB strength is presented. We build on the results of our initial report[17] as well as the aforementioned reports[27,40,41,53,54] that identify halogenated benzene derivatives as promoting significant XB interactions. Within our study, structural components such as the halogen identity and the presence of EWGs on the benzene ring of the XB donors are systematically investigated using both NMR spectroscopy and computational measurements. Somewhat unique to this study, structural parameters of the XB acceptors are also explored in a similar manner. While it is widely accepted that strong amine-based XB acceptors—for example, quinuclidine and DABCO—form adducts with XB donors,[27,40,53] herein we seek to expand measurements to other types of XB acceptors—notably molecules whose oxygen atom interacts with the XB donor's σ-hole—and identify structural parameters that promote XB as well as establish the impact of solvent on XB interactions.

2. METHODS

2.1. Materials and Instrumentation. All chemicals were purchased commercially (Millipore-Sigma, Oakwood Chemical, Fisher Scientific, TCI, and Strem Chemicals) and used without further purifications or modifications. A Bruker AVANCE III 400 NMR spectrometer was used to characterize the chemical shifts of XB donor and acceptor molecules as well as to monitor all NMR titrations of XB adducts.

2.2. Computational Methodology. Halogen bonds are difficult to properly characterize computationally as their interactions involve dispersion, electrostatics, and charge-transfer effects. In this study, density functional theory (DFT) was used to estimate the energy of interaction between XB donors and acceptors. Recent XB benchmarking studies[55−58] suggest that the M06-2X, ωB97-xD, and B3LYP-D3 functionals, when combined with a large basis set (cc-pVTZ), produce interaction energies and optimized geometries in closest agreement with CCSD(T)/cc-pVTZ results. CCSD(T) is often considered as the "gold standard" among coupled-cluster (CC) methods because of its inclusion of triple excitations, which is important to achieving satisfactory accuracy for non-covalent interactions such as XB.[55,59] There were fewer reports of XB basis set effects available in the literature, although Siiskonen and Priimagi[57] evaluated double-zeta (DZ) basis sets in comparison to CCSD(T)/CBS and found that the DGDZVP basis set offered the best performance and even outperformed some triple-zeta (TZ) basis sets. Given the accurate results reported in the literature with M06-2X, ωB97-xD, and B3LYP-D3, we performed functional and basis set benchmarking using the XB adduct IPFB−Me$_3$PO. This adduct was chosen as a model adduct because of its structural simplicity while still incorporating the important bonding motifs present in the other XB adducts that we were planning to study. For our reference calculation, we computed the geometries at the CCSD level with the cc-pVDZ (DZ) basis set and then refined the energetics using CCSD and CCSD(T) with the cc-pVTZ (TZ) basis set (Supporting Information, Table S1). In our benchmarking calculations, we included the hybrid functionals M06-2X, wB97xD, and B3LYP-D3, coupled with four different types of basis sets (cc-pVTZ//cc-pVDZ, def2-TZVP//def2TZV, 6-311++G(2d,p)//6-31+G(d), and DGDZVP) (Supporting Information, Table S1). The results of functional and basis set combinations were compared with CCSD(T)/cc-pVTZ//CCSD/cc-pVDZ results to determine the most effective methodological approach for XB calculations on non-model XB adducts. In all cases, the DFT interaction energies overestimate the CCSD(T)/cc-pVTZ//CCSD/cc-pVDZ interaction energies; however, in this study, we sought relative comparisons and not absolute energetic evaluations. To that end, a comparison between the computationally costly CCSD(T) results and the DFT results (Supporting Information, Table S1) caused us to choose the M06-2X functional for this study. We based that decision on our benchmarking results, as well as the confidence in the M06-2X functional reported in the literature.[55−58] Our basis set results on the model adduct (IPFB−Me$_3$PO) suggested that geometry optimizations using the cc-pVDZ basis set with CCSD would be sufficient, and we improved our energetic results by computation at the CCSD(T)/TZ level of theory, that is, M06-2X/cc-pVTZ//M06-2X/cc-pVDZ should provide reliable trends for all XB adducts in this study.

Gas-phase geometry optimizations and single-point calculations of the XB donors, XB acceptors, and XB adducts were performed using Gaussian16 software[60] with the M06 functional[61] and the cc-pVDZ[62] (geometry optimization) and cc-pVTZ[63] (single point) basis sets. For the larger atoms (iodine, bromine, and selenide), the small (28−e$^−$) Dirac−Fock (MDF) effective-core pseudopotentials and the corresponding basis sets were used.[64,65] Solvent-phase calculations were also performed using the polarizable continuum solvent model (PCM) at the M06-2X/cc-pVTZ//MO6-2X/cc-pVDZ level of theory.[66] Frequency analyses were conducted to confirm that the geometry-optimized structures corresponded to true minima (i.e., no imaginary frequencies) on the respective potential energy surfaces. The energy of interaction (ΔE_{int}) or binding energy between XB donors and acceptors was used to estimate the thermodynamic favorability and stability of the XB adducts. Specifically, more negative ΔE_{int} values suggest more thermodynamically favorable adducts. Zero-point energy and basis set superposition corrections were not included in the ΔE_{int} calculations based on the assumption that these harmonic corrections would be very similar for each system as the adducts are structurally similar. The XB bond lengths (X−B) and XB bond angles (R−X−B) of all XB adducts were also obtained as additional indicators of the strength of XB interactions. Specifically, strong XB interactions are typically characterized by bond lengths shorter than the van der Waals distances of the interacting atoms and nearly linear (180°) R−X−B bond angles.[8,32−34] All optimized geometries of XB adducts were visualized using the GaussView program.[67]

2.3. NMR Titrations. *2.3.1. NMR Sample Preparation.* As outlined in a tutorial review for NMR titration experiments by Thordarson,[50] extremely careful sample preparation, titrations conducted with a significant number of data points on well-defined molecular adducts, and repeated measurements are crucial to obtaining meaningful results. Herein, critical volumetric preparation of NMR titration samples was carried out using 1.00 mL 1/100 Mohr pipettes (Kimble, Class A), 10.0 μL microliter syringes (Hamilton Company), and 1.00 mL volumetric flasks (Wilmad-LabGlass) prior to transferring to 7 inch−5 mm NMR tubes (Wilmad) for titration measurements. For each sample, a set amount of the XB donor (in the range of 5.0−7.0 μL depending on the desired final concentration) was drawn via a microliter syringe into a volumetric flask and a specific amount of the XB acceptor, either weighed on an analytical balance or measured via a Mohr pipette, was subsequently added before carefully diluting the volumetric flask to volume with the solvent. Each mixture was then vortexed at 320 rpm for at least 25 s to fully dissolve all solids and mix the solution thoroughly prior to transferring to NMR tubes. Each titration experiment involves at least nine sequential samples, in which the concentration of the XB donor is kept constant (0.0475−0.0525 M depending on the donor−acceptor−solvent system), whereas the concentration of the XB acceptor is systematically increased from 0.0 M up to 5.0 M. For NMR titrations (see below), the highest concentration of the acceptor molecules was chosen to obtain a binding isotherm of at least 50% host saturation in each titration as reported in previous studies.[27,54]

2.3.2. NMR Titration Measurements. ^{1}H NMR and ^{19}F NMR spectra of halo(X)-benzene and halo(X)-pentafluorobenzene compounds (X = I, Br, and Cl) were recorded on a Bruker AVANCE III 400 NMR spectrometer at 400.13 and 376.46 MHz, respectively, with internal temperature set at

constant 298 K. All chemical shifts are reported in units of parts per million (ppm) relative to tetramethylsilane (TMS) for ^{1}H NMR and trichlorofluoromethane ($CFCl_3$) for ^{19}F NMR. All ^{1}H NMR samples were prepared in deuterated solvents, which acted as the lock and whose resonance peaks served as internal reference standards. ^{19}F NMR samples were prepared in protonated solvents with a sealed capillary tube containing 0.1 M trifluorotoluene in d_6-benzene, which both served as an internal reference standard ($\delta = -63.72$ ppm) and a deuterium lock signal.[27,40] All NMR titration experiments were carried out within 15 min of sample preparation.

2.3.3. Two-Dimensional NMR Measurements. 2-D ^{19}F$-^1$H HOESY spectra of XB adducts formed from mixtures of IPFB (0.0525 M) with excess XB acceptor molecules (tributylphosphine oxide (Bu_3PO)-0.7 M; trioctylphosphine oxide (Oct_3PO)-1.0 M) were obtained using a mixing time (d_8) of 800 ms to provide optimal signal-to-noise (S/N) ratios—see Section 3.4. The HOESY NMR spectra were collected using a Bruker AVANCE III NMR spectrometer with a nominal operating frequency of 400 MHz. The ^{19}F NMR signal was detected at 376.45 MHz, and each collected FID was the sum of 128 scans. The relaxation delay in between scans was 0.75 s. The spectral window for the directly observed ^{19}F NMR signal was 50 kHz wide (132.82 ppm) and the window was centered at -116.7 ppm. The t_2 time domain data was apodized with a 90°-shifted, squared sine bell with a maximum to minimum duration of 0.01024 s. A total of 512 complex points were collected in each FID using digital quadrature detection. A total of 200 FIDs were obtained (100 complex points in the t_1/f_1 dimension) using the States−TPPI method. The spectral window for the indirectly observed ^{1}H NMR signal was typically 2 ppm (800.3 Hz) and was centered at 1.4 ppm. The t_1 time domain data was zero-filled to a size of 1024 (512 complex). The t_1 time domain data was apodized with a 90°-shifted, squared sine bell with a maximum to minimum duration of 0.12495 s. Samples measured with HOESY were prepared in deuterated solvents to serve as a lock signal, degassed (N_2) to prevent O_2 interference, and transferred to screw-top NMR tubes (Wilmad-LabGlass) containing the same sealed internal reference capillary used for NMR titrations (Section 2.3.2). Quality control experiments for ^{19}F$-^1$H HOESY included measuring ^{19}F$-^1$H cross-coupling for *intramolecular* interactions in dexamethasone[68] as well as samples of the IPFB−quinuclidine adduct—a system featuring well-established strong *intermolecular* XB interactions more relevant to the described study.[40] 2D NMR spectra for both of these standard systems are provided in Supporting Information (Figures S1 to S3). To assess the reproducibility of the ^{19}F$-^1$H HOESY measurements, 2D NMR spectra of three dexamethasone samples were collected with intramolecular cross-peak intensities between the central F and H^1, H^7, H^{11}, H^{12}, and H^{14} exhibiting a percent relative uncertainty of 0.3 to 1.2% (Supporting Information, Figures S1 to S2). For each system, the molarity ratios of XB donor to XB acceptor were chosen to ensure at least 90% of donor is bound, in correspondence to a plateauing binding isotherm.

2.4. NMR Spectra/Data Analysis. All NMR spectra were analyzed using Mestrelab's MestreNova (v14.2) software. In ^{19}F NMR titrations, the chemical shift of interest progressively shifted upfield with increasing XB acceptor concentration. On the other hand, progressive downfield shifts were observed for ^{1}H NMR titrations with increasing XB acceptor concentration.

The XB interactions between donor−acceptor adducts were fast on the NMR time scale. The changes of ^{1}H and ^{19}F chemical shifts of the substituents of interest as a result of increasing acceptor concentration, indicative of XB interactions, were modeled in 1:1 binding isotherm plots as previously demonstrated in the literature.[27,40,54,69] Non-linear regression analyses were performed to yield relevant equilibrium K_a of the adducts, a representation of XB strength, based on the two following equations[40,50,70] (additional parameters and usage are described in Supporting Information, p. 7)

$$\Delta\delta = (\delta_{max} - \delta_o)\frac{[DA]}{[D_o]} \tag{1}$$

$$[DA] = \frac{1}{2}[[D_o] + [A_o] + \frac{1}{K_a} \\ - \sqrt{\left([D_o] + [A_o] + \frac{1}{K_a}\right)^2 - 4[D_o][A_o]}] \tag{2}$$

All regression analyses to determine K_a values were performed using an in-house designed Python code (Supporting Information, pp. 8−12) that was based on eqs 1 and 2 as well as curve-fitting methods reported in the literature for similar measurements.[40,50,70] The Python program reports additional data concerning the binding isotherms not provided by other reported methods, such as the percentage of XB donor that is bound and predicted δ_{max} (eq 1), and facilitates more efficient data transfer. For validation, all analyses conducted with the Python program were compared to results using http://supramolecular.org methodology developed by Thordarson.[50]

3. RESULTS & DISCUSSION

Prior experimental and computational research[17,40] has established that halogen-substituted arenes and perfluoroarenes (Figure 1) are able to act as XB donors and to promote
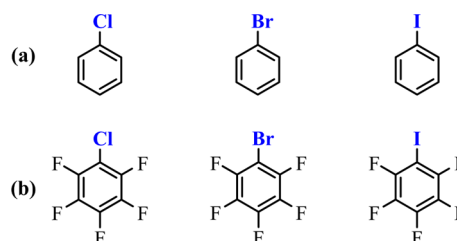

Figure 1. Studied XB donors of (a) halobenzenes and (b) haloperfluorobenzenes.

XB interactions with various XB acceptor molecules. Effective aromatic XB donors typically feature a halogen atom at position 1, where the σ-hole is established, and allows for tuning the size of the σ-hole and the corresponding XB donor strength by varying the functional groups at other ring positions. This versatility enables strategic design of molecular structure and subsequent incorporation of XB interactions into a variety of systems for potential applications. These halogen-substituted arenes form the basis of our study exploring XB interaction strength as a function of *both* XB donor and acceptor molecular strength.

3.1. XB Donor Structure—Halogen Effect and Electron Withdrawing Groups.

3.1.1. DFT Analysis (XB Donors). Halogen-monosubstituted arenes (Figure 1a) are predicted to exhibit σ-hole sizes that are dependent on the size and polarizability of the halogen atom, as shown by the molecular electrostatic potentials (MEPs) in Figure 2A, which
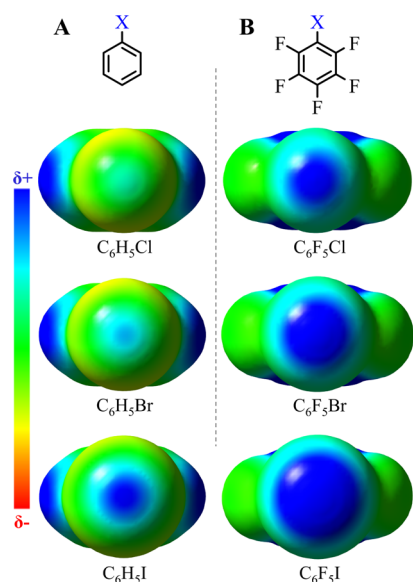

Figure 2. MEP diagrams illustrating the σ-hole in (A) 1-halobenzenes (left) and (B) 1-halopentafluorobenzenes with 2,3,4,5,6-pentafluoro substitution (right) for XB donors where X is varied from Cl to Br to I (top-to-bottom).

are consistent with other modeling of these compounds in the literature.[17] Similarly, perfluoro-substituted analogues of the XB donors (Figure 1b) exhibit larger, more electron-deficient σ-holes with the addition of EWGs at the *ortho*, *meta*, and *para* positions of the ring (Figure 2B). While not as e⁻-withdrawing as nitro or carbonyl groups, fluorine EWGs do not engage in non-XB interactions such as dipole−dipole interaction and HB with common XB acceptors and/or solvents while still promoting the formation of a substantial σ-hole for XB interactions.[17] In both cases, quantum calculations show that the size of the σ-hole corresponds to the polarizability of the halogen atom (I > Br > Cl). When EWGs are added to the aromatic ring, e⁻ density is further pulled away from the crown of the interacting halogen, creating a larger σ-hole with stronger interactions with XB acceptors.

DFT was used to examine each XB donor species (Figure 1) interacting with tributylphosphine oxide (Bu₃PO)—an established XB acceptor molecule.[40,54] Three computationally determined structural metrics were used to evaluate the strength of XB interactions: interaction energies (ΔE_{int}), XB bond length/distance (XBD), and R−X−B bond angle (θ). Because the σ-hole is generated along the bonding axis, more negative ΔE_{int}, shorter XBD distances, and more linear θs (approaching 180°) are all considered as indicators of strong XB adducts.[8,32−34] Figure 3 shows a representative geometry-optimized XB adduct of the XB donor IPFB, which exhibited the largest σ-hole (Figure 2B, bottom), and Bu₃PO, the common XB acceptor. This adduct has an XBD of 2.74 Å and a θ of 175.9°, suggesting significant XB interaction. Geometry-optimized XB adducts for all XB donors with the common XB acceptor Bu₃PO are provided in Supporting Information
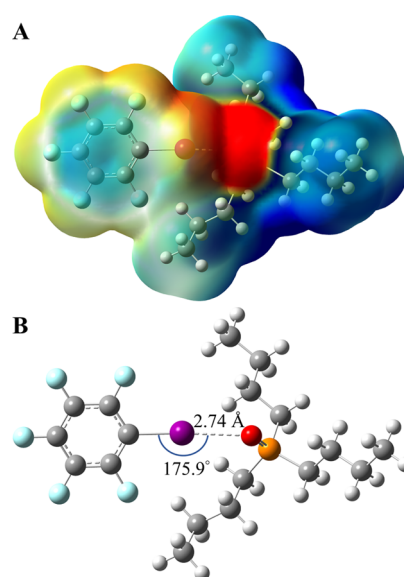

Figure 3. (A) Space-filled electrostatic potential and (B) geometry-optimized XB adduct of IPFB (XB donor) with Bu₃PO (XB acceptor) with XB bond length and C−I−O bond angle indicated. Note: Geometry-optimized XB adducts for all systems tested can be found in Supporting Information (Figures S4−S7 and S41−S52).

(Figures S4 to S7). Also in Figure 3 is an MEP for the representative IPFB−Bu₃PO adduct demonstrating significant e⁻ density being directed from the oxygen atom on the phosphine oxide into the σ-hole on the iodine atom of the XB donor. Interaction energies (ΔE_{int}) for various XB donors interacting with Bu₃PO are listed in Table 1 and suggest that

Table 1. Experimental K_a Values and M06-2X/cc-pVTZ// M06-2X/cc-pVDZ Interaction Energies (ΔE_{int}), Bond Distances (XBD), and Bond Angles of XB Adducts of XB Donors and XB Acceptor Bu₃PO

XB donors	ΔE_{int} (kcal/mol)[a]	X−B distance (Å)	R−X−B angle (θ)	K_a (M⁻¹)[b]
Halobenzene				
chlorobenzene	−4.06	2.99	165.5	0.77 (± 0.02)ₙ₌₃
bromobenzene	−4.74	2.94	172.9	0.98 (± 0.05)ₙ₌₃
iodobenzene	−7.00	2.91	174.7	1.48 (± 0.03)ₙ₌₃
Haloperfluorobenzene				
Cl-PFB	−6.27	2.83	164.7	2.84 (±0.10)ₙ₌₃
Br-PFB	−7.86	2.77	175.9	3.36 (±0.08)ₙ₌₄
I-PFB	−10.95	2.74	175.9	22.08 (±1.02)ₙ₌₄

[a]$\Delta E_{int} = E(XB\ adduct) − [E(XB\ donor) + E(XB\ acceptor)]$ (gas-phase values). [b]Determined from non-linear regression modeling of 1:1 binding isotherms collected during NMR titrations in cyclohexane; italicized K_a values indicate non-plateauing binding isotherms as a result of non-specific (non-XB) intermolecular interactions. Computational interaction energies, bond distances, and bond angles of the control adducts of all XB donors and hexane are included in Supporting Information (Figures S8−S9).

the strength of XB donors tracks with the σ-hole size. As the σ-hole becomes more prominent moving from chloro- to iodo-substitution of either the halobenzene or the perfluoro-analogue, ΔE_{int} values become more negative, XBD values decrease, and θ values approach 180°. The trends observed are consistent with a previous study examining dihalobenzene with

and without EWGs interacting with a non-aromatic explosive molecule.[17] As a control, the same XB interactions were tested with hexane, a non-XB acceptor, and showed comparatively negligible interaction energies (Supporting Information, Figures S8 to S9).

It is important to note that in the Jaini et al. study, the DFT analysis was performed in the gas phase.[17] In an expansion to that prior work, a major facet of this study is to experimentally explore the XB interactions for these systems *in solution.* Solvent-phase calculations on systems of the size and complexity as used in this study are computationally costly and so the bulk of our computational results presented below were performed in the gas phase. However, we did explore the effects of solvent using the PCM implicit solvent model on the model compound IPFB–Bu$_3$PO. This system was chosen to capture the physical nature of the organic R substituents as well as to have a direct comparison with the molecular systems used in the experimental solvent study described in Section 3.3. As shown in Figure S10 and Table S2 of Supporting Information, the inclusion of various solvents (cyclohexane, benzene, carbon tetrachloride, diethyl ether, and chloroform) does not significantly affect the optimized XB geometries (i.e., XB bond lengths decrease by 0.02 Å and R–X–B angles change by less than 1.5°). Energetically, and relative to the gas-phase results, solvent screening only reduces the interaction energies (ΔE_{int}) by less than 1.40 kcal/mol for low dielectric solvents (cyclohexane, benzene, and carbon tetrachloride) and by less than 2.50 kcal/mol for the more polar solvents (diethyl ether and chloroform). In all cases, the dominant interaction between IPFB and Bu$_3$PO is the XB interaction.

3.1.2. NMR Titration Analysis of Solution XB (XB Donors). For solution-based experiments, NMR titration provides an established tool for characterizing the strength of XB interactions between XB donors and acceptors.[27,40] Specifically, the halogen-monosubstituted arene XB donors and their perfluorinated counterparts, whose concentrations are kept constant, are mixed in solution with increasing concentrations of Bu$_3$PO, while ^{1}H or ^{19}F NMR spectra are collected, respectively. Upon the formation of XB adducts of the two molecules, measurable NMR signal shifts should be observed for the hydrogen or fluorine atoms on the XB donors' aromatic rings. ^{1}H and ^{19}F NMR shifts of atoms *ortho* to the halogen atom at position 1 of halo-benzene and halo-pentafluoroben-zene compounds, respectively, are then monitored as a function of systematically increasing XB acceptor concen-tration. These shifts can be plotted as a function of XB acceptor concentration to yield binding isotherms (i.e., titration curves), from which the association constant (K_a) of the XB adducts can be derived. The magnitude of K_a reflects either the strength of a specific XB interaction or can provide evidence of the presence of non-specific interactions.[71] Binding isotherms that exhibit sharp plateaus as the XB donor becomes saturated with the XB acceptor indicate a more specific, stronger XB interaction while those that do not plateau represent systems where non-specific, transient interactions (non-XB interactions) are more substantial.[71] Furthermore, plateauing binding isotherms that increase more sharply after the first few increases of XB acceptor concentration generally correlate to higher K_a values and thus represent stronger XB interactions. ^{19}F NMR spectroscopy is particularly well-suited for this type of measurement due to its high sensitivity that stems from the ^{19}F isotope's 100% natural abundance and the inherently clean spectra of the technique.[72] Initial ^{1}H and ^{19}F

NMR spectra for all of the XB donor molecules (Figure 1) in cyclohexane are included in Supporting Information (Figures S11–S14) for reference.

Figure 4 illustrates a representative example of an NMR titration experiment used for K_a determination as an indicator
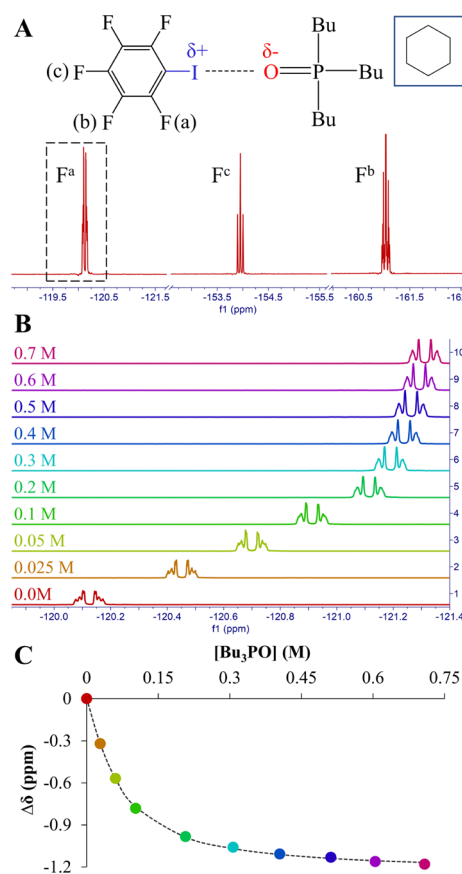

Figure 4. Representative NMR titration experiment for XB donor IPFB (0.0525 M) titrated with XB acceptor Bu$_3$PO including (A) initial ^{19}F NMR spectrum of IPFB prior to titration, (B) change in the *ortho* F resonance shifts during the addition of increasing concentrations of Bu$_3$PO, and (C) corresponding binding isotherm used for non-linear regression analysis and determination of the K_a that reflects XB interaction strength of the adduct (solvent: cyclohexane).

of the strength of XB interaction. In this example, the ^{19}F NMR spectra are collected for XB adducts of IPFB with Bu$_3$PO as the concentration of the latter XB acceptor is varied relative to IPFB concentration. Figure 4A shows an expanded ^{19}F NMR spectrum prior to the addition of XB acceptor molecules with chemical shifts indicated for the *ortho* (−120.13 ppm), *para* (−153.95 ppm), and *meta* (−161.04 ppm) fluorine atoms. With the addition of Bu$_3$PO and the formation of the XB donor−acceptor adducts, progressively more upfield shifts are observed (Figure 4B) for fluorine resonances. This trend is consistent with the literature reports[27,51] as upfield shifts ($\Delta\delta$) of fluorines are expected when e$^-$ density is directed into the σ-hole via XB and subsequently shields the fluorine atoms from the NMR magnetic field. The $\Delta\delta$ is then plotted as a function of Bu$_3$PO concentration to form a titration curve or binding isotherm (Figure 4C) that can be fitted to extract a K_a value reflective of the strength of XB interaction (see Section 2.4 of

Methods). Analogous ^{1}H NMR experiments can be conducted to determine K_a for the halobenzene XB donors with the same XB acceptor (i.e., Bu$_3$PO).

The K_a derived from NMR titrations for all the tested XB donors (Figure 1) with Bu$_3$PO are summarized in Table 1 alongside the previously discussed DFT results with representative examples of each titration experiment provided in Supporting Information (Figures S15−S20). The data informs about both the halogen dependence and the importance of EWGs in the XB donor structure toward XB strength. The K_a values for halobenzene XB donors suggest that these donor molecules do not engage in significant XB interactions when in solution. The strength of XB interactions engaged by iodobenzene (K_a = 1.48 M^{-1}) does not differ significantly from that of either bromobenzene (K_a = 0.98 M^{-1}) and/or chlorobenzene (K_a = 0.77 M^{-1}). These low K_a values were derived from non-plateauing binding isotherms that are consistent with the presence of non-specific (non-XB) interactions.[71] This result is reinforced by Otte et al. (2021) that suggests that iodobenzene can engage in XB and two other non-XB interactions with the XB acceptor quinuclidine.[52] As seen in the titration data for the perfluorinated XB donors (Table 1), it is the addition of EWGs (i.e., fluorines) in the substituent positions of the benzene ring that results in plateauing binding isotherms (Supporting Information, Figures S18−S20) and the derivation of meaningful K_a values. However, even with the addition of fluorine to the donor structure, a dramatic, order-of-magnitude increase in average K_a (22.08 M^{-1}) is observed only with IPFB acting as the XB donor. While a preference for IPFB was expected, the marked difference seen experimentally was not predicted by the gas-phase computational results (Table 1), which suggest a gradual strengthening of the XB interactions as the halogen increased in size and as EWGs were added to the aromatic ring. In solution-based systems, it appears that the XB donor structure requires *both* the iodine substitution as well as the presence of EWGs for the σ-hole to promote significant XB interactions. These collective results indicate that the solvent is likely to play a prominent role in the strength of XB interactions as is addressed experimentally later in this study.

3.2. XB Acceptor Structure—R Group, Central Atom, and Lewis-Base Atom Engaged with the σ-Hole. A less frequently studied aspect of XB interactions is the effects of XB acceptor structure on XB interactions. Herein, we measured both experimentally and computationally the strength of XB interactions between the strongest XB donor from our measurements (i.e., IPFB) and various XB acceptors with different structural parameters. As shown in the scheme of Figure 5A,B, a number of structural motifs of XB acceptor molecules were targeted for investigation including variations to the central atom (CA), the R groups attached to the CA, and the Lewis-base atom (:B) that is doubled bonded to the central atom and directly interacting with the σ-hole of the XB donor. For all the cases that follow herein, representative NMR titration results for each system along with DFT geometry optimizations are provided in Supporting Information (Figures S20−S52). The overall goal of this part of the study was to identify structural parameters that impact the formation of the XB adducts and the corresponding Lewis basicity (δ−) of the XB acceptors.

3.2.1. DFT and NMR Analysis of XB Acceptors—Central Atom. In order to gain more insight into the structural features of XB, we performed M06-2X/cc-pVTZ/M06-2X/cc-pVDZ
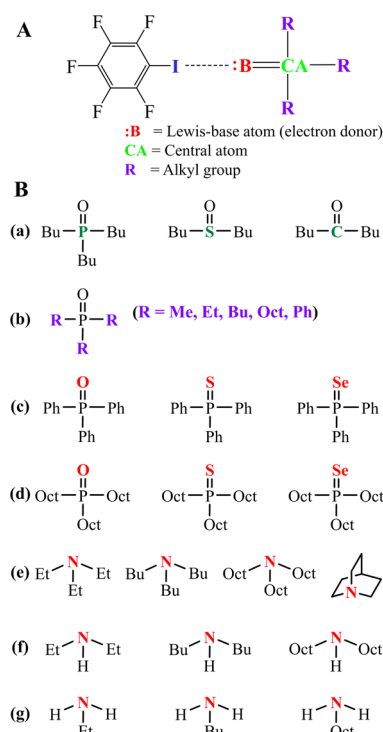

Figure 5. (A) Structural schematic of XB acceptors used in this study. (B) Specific XB acceptors with structures that systematically vary the (a) central atom, (b) R group, (c,d) Lewis-base atom directly engaging with the XB donor's σ-hole, (e) tertiary, (f) secondary, and (g) primary amines.

calculations using the XB donor IPFB and a variety of XB acceptors (Figure 5 and Table 2). Using Bu$_3$PO as a starting point, the first set of experiments varied the central atom from phosphorus to sulfur and then to carbon while monitoring the impact on XB interactions with IPFB (Figure 5B-a). According to the DFT results (Table 2), phosphorus (P) and sulfur (S) serving as the central atom resulted in significant XB interactions (ΔE_{int} = −10.95 kcal/mol and −8.22 kcal/mol, respectively) and smaller XBDs (2.74 Å). Comparatively, less negative ΔE_{int} and larger XBD (−5.94 kcal/mol and 2.93 Å) were recorded with carbon (C) as the central atom. When the interaction is analyzed in solution via NMR titrations, the XB strength tracks that of the gas-phase computational data (P > S > C), but the presence of solvent leads to a notable decrease in interaction strength. For example, the K_a (22.08 M^{-1}) associated with a central P drops precipitously to 5.23 and 0.46 M^{-1} when the central atom is S and C, respectively. Notably, the titration curve for the carbon-centered XB acceptor interacting with IPFB does not plateau, suggesting that the interactions between the two molecules are more transient and non-specific.

Collectively, these experimental and computational results suggest two influences concerning the central atom on the XB acceptor that ultimately affect the magnitude and effectiveness of the Lewis basicity (δ−) region: electronegativity (EN) and atomic radii. Phosphorus has a lower EN (∼2.1) than both sulfur and carbon (EN ≈ 2.5), allowing the double-bonded oxygen atom to attract more e$^-$ density and enhance the XB acceptor strength of the P═O moiety. Moreover, the significant drop in K_a between the two XB acceptors possessing central atoms of similar EN, Bu$_2$SO and Bu$_2$CO, suggests that the polarizability of the central atom may also play a role.

Table 2. Experimental K_a Values and M06-2X/cc-pVTZ//M06-2X/cc-pVDZ Interaction Energies (ΔE_{int}), Bond Distances (XBD), and Bond Angles of XB Adducts Using the XB Donor IPFB with Various XB Acceptors

XB Acceptors	ΔE_{int} (kcal/mol)[a]	X–B distance (Å)	R–X–B angle (θ)	K_a (M^{-1})[b]
Control Adduct				
Hexane	−0.19	3.46	179.3	control (*no shift*)
Varying Central Atoms				
Bu$_3$**P**O	−10.95	2.74	175.9	22.08 (± 1.02) $_{n=4}$
Bu$_2$**S**O	−8.22	2.74	178.2	5.23 (± 0.40) $_{n=2}$
Bu$_2$**C**O	−5.94	2.93	174.7	*0.46 (± 0.01)* $_{n=2}$
Varying R Groups				
Me$_3$PO[#]	−9.15	2.73	176.4	4.85 (± 0.31) $_{n=2}$
Et$_3$PO[#]	−9.84	2.73	177.4	2.80 (± 0.16) $_{n=2}$
Bu$_3$PO[#]	−10.95	2.74	175.9	5.66 (± 0.15) $_{n=2}$
Oct$_3$PO[#]	−13.49	2.79	163.2	14.24 (± 2.03) $_{n=2}$
Ph$_3$PO[#]	−8.90	2.76	178.6	3.82 (± 0.17) $_{n=2}$
Varying Lewis-Base Atoms				
Oct$_3$P**O**	−13.49	2.79	163.2	44.02 (± 1.02) $_{n=3}$
Oct$_3$P**S**	−12.28	3.38	162.9	6.07 (± 0.34) $_{n=2}$
Oct$_3$P**Se**	−11.99	3.51	168.5	16.54 (± 2.06) $_{n=2}$
Ph$_3$P**O**[#]	−8.90	2.76	178.6	3.82 (± 0.17) $_{n=2}$
Ph$_3$P**S**[#]	−7.82	3.40	174.6	--[c]
Ph$_3$P**Se**[#]	−7.81	3.53	178.7	--[c]

[a]$\Delta E_{int} = E(\text{XB adduct}) - [E(\text{XB donor}) + E(\text{XB acceptor})]$ (gas-phase values). [b]Determined from non-linear regression modeling of 1:1 binding isotherms collected during NMR titrations in cyclohexane (unless otherwise noted). [#]System tested in benzene; italicized K_a values indicate non-plateauing binding isotherms as a result of non-specific (non-XB) intermolecular interactions. [c]Result is inconclusive as maximum $\Delta\delta$ is <0.2 ppm during titration (~0.007 ppm).

Atoms with larger polarizability [P (25 au) > S (19.4 au) > C (11.3 au)][73] possess larger, more diffuse, and more polarizable e$^-$ clouds that are more easily drawn toward the oxygen atom, conferring higher e$^-$ density and thus imparting stronger Lewis basicity (i.e., stronger XB acceptor) toward the oxygen. In this case, phosphorus enjoys a more optimal EN and more polarizable e$^-$ density than sulfur and carbon, which explains the significantly higher K_a of Bu$_3$PO. It is notable that the additional valency and extra alkyl R group in Bu$_3$PO adds additional e$^-$ density to phosphorus that is subsequently drawn away toward the oxygen involved in XB interactions. These factors collectively increase the e$^-$ density on the oxygen atom on the XB acceptor and thus strengthen the XB interaction, suggesting that the presence and nature of electron-donating alkyl groups on the central atom of an XB acceptor is integral to XB strength.

3.2.2. DFT and NMR Analysis of XB Acceptors—R Group. To further explore the nature of alkyl group substitution at the central atom of the XB acceptor (Figure 5A), we computed optimized geometries and interaction energies with IPFB (Table 2) where the phosphine oxide moiety (**R**$_3$PO) is substituted with various R groups such as methyl, ethyl, butyl, octyl, and phenyl (Figure 5B-b). As the number of methylene units in the R group is increased (i.e., methyl to octyl) and

assuming a *trans* conformation, ΔE_{int} becomes more favorable (i.e., more negative), indicating increasingly stronger XB interactions between the molecules. These results suggest that the presence and length of the alkyl groups can stabilize the interaction. For the solution-phase experimental analysis of these systems, solubility issues required the use of benzene as a common solvent for all the measurements[a]. K_a values measured using NMR titration for these systems (Table 2) show notable and comparable XB interaction strength between IPFB and R$_3$PO when R is methyl (4.85 M^{-1}), ethyl (2.80 M^{-1}), butyl (5.66 M^{-1}), or phenyl (3.82 M^{-1}). A notable exception to this trend in XB strength is observed for IPFB with Oct$_3$PO, which exhibits an anomalously high K_a value of 14.24 ± 2.03 M^{-1}. While the reasons for this type of XB with a long hydrocarbon R group are not entirely understood, it can be hypothesized that the flexibility of the longer aliphatic chains allows for a greater degree of interaction with the XB donor and subsequently strengthens the primary XB interaction between iodine (σ-hole) and oxygen. This hypothesis is tested further with two-dimensional NMR experiments described below (Section 3.4). Additionally, from Table 2, the difference in K_a measured for the same system (Bu$_3$PO with IPFB) in two different solvents is notable: 22.04 M^{-1} in cyclohexane *versus* 5.66 M^{-1} in benzene. This

result, again, suggests that solvent is a fundamental factor that impacts XB interaction (Section 3.3).

3.2.3. DFT and NMR Analysis of XB Acceptors—Lewis-Base Atom. The third major structural parameter of the XB acceptor that was explored was the impact of the Lewis-base atom (:B) that is double-bonded to the central atom and directly engaged with the σ-hole of the XB donor (Figure 5A). In this case, a limited supply of commercially available, air-stable compounds existed which consequently limited the number and type of experiments that could be conducted. Two sets of molecules were ultimately identified for studying the role of the Lewis-base atom (Figure 5B-c,d): trioctyl- and triphenyl-phosphine oxides, sulfides, and selenides. DFT analysis of the $Oct_3P\!\!=\!\!B$: compounds, where B: was varied (O, S, and Se), showed systematically more negative ΔE_{int} (stronger XB interactions) and smaller XBDs moving from selenium through sulfur and to oxygen (Table 2). A similar trend in calculations, albeit smaller in magnitude, was observed for the phenyl systems ($Ph_3P\!\!=\!\!B$) as well. In both cases, the most negative ΔE_{int} and smallest XBD were recorded for the oxides.

NMR titrations of the $Oct_3P\!\!=\!\!B$: compounds with IPFB were tested in cyclohexane while titrations of the $Ph_3P\!\!=\!\!B$: compounds with IPFB were tested in benzene. Given the strength of XB previously reported for IPFB with Bu_3PO (K_a = 22.08 M^{-1}), with oxygen serving as the Lewis-base atom and the established trend of octyl groups stabilizing the XB interactions, it is relatively unsurprising that the highest average K_a value (44.02 M^{-1}) of any system in the study is IPFB interacting with Oct_3PO (in cyclohexane) (Table 2). NMR titration of IPFB with the two other octyl-substituted compounds, Oct_3PS and Oct_3PSe, resulted in K_a values of 6.07 and 16.52 M^{-1}, respectively (in cyclohexane), both of which indicate a significant degree of XB interaction. Because all the systems have the same R group (i.e., octyl), the differences in measured K_a values can be attributed to the identity of the :B atom and establish that the Lewis-base atom also plays a significant structural factor in the strength of XB acceptors. Two structural factors that seemingly impact the ability of the Lewis-base atom to donate electrons include EN and atomic polarizability. Oxygen, sulfur, and selenium have ENs of 3.44, 2.58, and 2.55 and atomic polarizabilities of 5.3 au, 19.4 au, and 28.9 au, respectively.[73] The higher K_a and more negative ΔE_{int} values of $R_3P\!\!=\!\!O$ compounds suggest that even though O does not have as diffuse of an e^- cloud as S and Se do (as a result of their higher respective atomic polarizabilities), its high electronegativity allows it to draw a larger amount of e^- density from P that subsequently leads to stronger Lewis-base capability and XB acceptor strength. It also appears that the high electronegativity of oxygen does not significantly hinder its ability to donate electrons to the σ-hole in comparison to sulfur and selenium. As S and Se share comparable ENs, the notable difference in K_a values between their respective XB acceptors can be explained by their atomic polarizabilities: selenium with higher polarizability has a more diffuse e^- cloud and can donate more e^- density to the σ-hole of the XB donor IPFB. The strength of the selenium-containing compound is not unprecedented as its analogue, Ph_3PSe, was shown to exhibit significant XB interactions with diiodotetrafluorobenzene during crystallization studies.[74] Other selenide and sulfide molecules have also been reported to form crystals through strong XB interactions with 1,4-diiodotetrafluorobenzene and 1,4-dibromotetrafluorobenzene.[75] In the same study, Cherny-sheva and co-workers observed that selenium-containing XB acceptors appear to engage in stronger XB with XB donors than their sulfur-containing counterparts.[75]

Another aspect of the data collected in this section is the ability to compare two systems varying only by the R group: $Oct_3P\!\!=\!\!B$: versus $Ph_3P\!\!=\!\!B$:. Experiments of IPFB with XB acceptors featuring the phenyl group with O, S, and Se as the Lewis-base atom show either lower K_a values (3.82 M^{-1} for Ph_3PO) or negligible changes of NMR chemical shifts during titrations for indefinite K_a measurements (Table 2). Such a result reinforces our prior findings that show the critical role of R group on XB strength: longer, more flexible aliphatic chains such as the octyl group stabilize the XB strength while conjugated groups such as phenyl appear to hinder XB acceptor capability.

3.2.4. DFT and NMR Analysis of XB Acceptors—Amines. A logical extension of the Lewis-base atom study is to test interactions of IPFB with nitrogen-based XB acceptors where nitrogen serves as both the central atom *and* the Lewis-base atom with more favorable R groups (e.g., octyl and butyl groups) attached to the nitrogen (Figure 5B-e−g). Sarwar et al. previously used NMR titrations to show K_a for adducts of IPFB and nitrogen-based XB acceptors varying from very weak interactions (IPFB−triethylamine, $K_a \approx 1.3$ M^{-1}) to rather strong (IPFB−quinuclidine, $K_a \approx 20$ M^{-1})—an early indicator of the impact of R groups on XB interaction strength.[40] For our study, IPFB was complexed with a range of tertiary (Et_3N, Bu_3N^b, Oct_3N, and quinuclidine), secondary (Et_2NH, Bu_2NH, and Oct_2NH), and primary amines ($EtNH_2$, $BuNH_2$, and $OctNH_2$). DFT analysis of these interactions is summarized in Table 3. In general, nearly all the amines interacting with IPFB resulted in ΔE_{int} values between −7.25 and −8.97 kcal/mol with XBDs in the range of 2.8−3.0 Å, which are indicative of XB interactions. The lone exception for this set of experiments was the interaction of IPFB with quinuclidine which DFT calculations showed to have the most negative ΔE_{int} and smallest XBD of the entire set at −11.41 kcal/mol and 2.77 Å, respectively.

The results of NMR titration experiments are included in Table 3 and show that secondary amines are slightly stronger XB acceptors than tertiary and primary amines, a result of the balance between inductive stabilization and steric hindrance known to occur in secondary amines—in agreement with the Metrangolo et al. study.[76] The strength of amine-based XB acceptors, except quinuclidine, is comparable and weak, suggesting that favorable R groups (i.e., butyl and octyl) do not significantly enhance XB acceptor strength. In fact, the R groups of these amine-based XB acceptors are free to rotate and sterically limit the exposure of nitrogen's lone pair of electrons to IPFB, thus decreasing the strength of these XB acceptors. On the other hand, quinuclidine, a bicyclic amine, is less sterically hindered than the other three tested tertiary amines because its R groups are rigidly "pulled" back to expose more of nitrogen's lone pair of electrons for donating to IPFB.

3.3. Solvent Effects on XB Interactions. In addition to XB donor and acceptor structural properties, one of the recurring observations that can be ascertained from our results is that the presence and choice of solvent affects the strength of XB interactions and warrants dedicated study. The influence of solvent in the strength of XB interactions has been explored in the scientific literature but has resulted in varying conclusions. This is largely because of the limited number of solvents included in most studies[53,54] or because the system used to

Table 3. Experimental K_a Values and M06-2X/cc-pVTZ// M06-2X/cc-pVDZ Interaction Energies (ΔE_{int}), Bond Distances (XBD), and Bond Angles of XB Interactions of XB Donor IPFB and XB Acceptors

XB acceptors	ΔE_{int} (kcal/mol)^a	X—B distance (Å)	R—X—B angle (θ)	K_a (M^{-1})^b
Tertiary Amines				
Et$_3$N	−8.93	2.85	179.6	1.61 ($\pm$0.02)$_{n=2}$
Bu3N	−7.25	2.99	178.7	0.66 ($\pm$0.03)$_{n=2}$
Oct3N	−7.26	2.98	179.1	1.19 ($\pm$0.08)$_{n=2}$
quinuclidine	−11.41	2.77	179.9	25.60 ($\pm$0.48)$_{n=2}$
Secondary Amines				
Et$_2$NH	−8.75	2.84	179.0	1.59 ($\pm$0.07)$_{n=2}$
Bu2NH	−8.88	2.84	179.2	2.14 ($\pm$0.10)$_{n=2}$
Oct2NH	−8.97	2.84	179.4	3.52 ($\pm$0.20)$_{n=2}$
Primary Amines				
EtNH$_2$	−8.23	2.85	177.8	N/A^c (gas)
BuNH$_2$	−8.28	2.85	177.8	1.40 ($\pm$0.06)$_{n=2}$
OctNH2	−8.33	2.85	177.6	1.90 ($\pm$0.05)$_{n=2}$

$^a\Delta E_{int} = E$(XB adduct) − [E(XB donor) + E(XB acceptor)] (gas-phase values). ^{b}Determined from non-linear regression modeling of 1:1 binding isotherms collected during NMR titrations in cyclo-hexane. ^{c}No NMR titration was performed because pure ethylamine (EtNH$_2$) exists in gas phase.

evaluate solvent effects exhibited weak XB interactions that it made the impact of solvent less observable (e.g., iodoper-fluorooctane with triethylamine exhibiting a K_a range of 0.3– 2.8 M^{-1} in various solvents).[40] After reporting the first XB iodoperfluoroalkane−amine adduct (i.e., iodoperfluoropropane with quinuclidine), Messina et al.[77] used ^{19}F NMR to examine XB interactions of dihalotetrafluoroethane in various solvents to show how XB is impacted by the presence of solvents with heteroatoms (N > S ≥ O) and by steric effects. Cabot and Hunter tested XB between iodoperfluorohexane and a range of amine-based XB acceptor molecules in three different solvents (C$_6$H$_6$, CCl$_4$, and CHCl$_3$) and measured K_a values (0.5–30 M^{-1}) that suggested XB is largely an electrostatically driven interaction.[54] Sarwar et al. provided an important contribution for understanding solvent effects on XB with a theoretical evaluation and experimental K_a measurements of C$_8$F$_{17}$I (XB donor) with triethylamine (XB acceptor) in a diverse array of solvents of varying polarity that showed a range of smaller K_a values (0.3–2.8 M^{-1}). In general, Sarwar and co-workers reported a relatively minor XB dependence on solvent polarity, but a substantial diminishment of XB strength in HB-capable solvents (e.g., *tert*-butyl alcohol, chloroform, and 2-prop-anol).[40] More recently, the concept of competing XB *versus* HB interactions was explored with the self-assembly of crystals by Robertson and co-workers,[27] who reported more dominant HB in less polar solvents, whereas XB was favored in more polar solvents. Recognizing that solvent effects would involve more than just polarity, an important part of Sarwar et al. study was relating the solvent effects on XB interactions with

established solvent polarity parameters and indices.[40] This type of interpretation, which is pursued in our study as well, acknowledges the concept of competing interactions in an organized manner, thereby expanding both our understanding of XB in different solvents as well as its broader use in chemical applications (e.g., separation science).[10,11]

NMR titrations were performed with IPFB interacting with Bu$_3$PO (a strong XB adduct) in various solvents including cyclohexane, dichloromethane, chloroform, *p*-xylene, toluene, benzene, carbon tetrachloride, diethyl ether, acetonitrile, tetrahydrofuran, and triethylamine. The chosen XB donor− acceptor adduct for the solvent study (IPFB−Bu$_3$PO) exhibited a K_a value of 22.08 M^{-1}, 8-fold stronger than the system tested by Sarwar et al. (iodoperfluorooctane with triethylamine). The NMR-measured K_a values of IPFB interacting with Bu$_3$PO as a function of solvent are listed in Table 4 along with typical dipole moment and dielectric

Table 4. Experimental K_a Values of the IPFB−Bu$_3$PO Adduct in Various Solvents

solvent	K_a (M^{-1})^a	dipole moment[78] (debye; D)	dielectric constant[78] (F/m)	Snyder index[83]
cyclohexane	22.08 ($\pm$1.02)$_{n=4}$	0.0	2.02	0.0
dichloromethane	0.60 ($\pm$ 0.01)$_{n=2}$	3.8	8.93	3.4
chloroform	--^{b}	3.8	4.89	4.4
p-xylene	8.42 ($\pm$0.42)$_{n=2}$	0.0	2.27	2.4
toluene	6.23 ($\pm$0.21)$_{n=2}$	1.0	2.38	2.3
benzene	5.66 ($\pm$0.15)$_{n=2}$	0.0	2.27	3.0
carbon tetrachloride	4.18 ($\pm$0.10)$_{n=2}$	0.0	2.24	1.7
diethylether	7.99 ($\pm$0.15)$_{n=2}$	3.8	4.20	2.9
acetonitrile	1.65 ($\pm$ 0.05)$_{n=2}$	13.0	35.94	6.2
tetrahydrofuran	6.11 ($\pm$0.46)$_{n=2}$	5.8	7.58	4.2
triethylamine	1.51 ($\pm$0.18)$_{n=2}$	2.2	2.42	1.8

^{a}Determined from non-linear regression modeling of 1:1 binding isotherm collected during NMR titrations; italicized K_a values indicate non-plateauing binding isotherms as a result of non-specific (non-XB) intermolecular interactions. ^{b}Result is inconclusive as maximum $\Delta\delta$ is <0.2 ppm during titration (0.12 ppm).

constant properties of each solvent. Initial ^{19}F NMR spectra of IPFB in other non-cyclohexane solvents as well as representative titration results for the IPFB−Bu$_3$PO adduct in the various solvents are provided in Supporting Information (Figures S53–S66). It should be noted that HB-donor solvents such as alcohols were purposely not included in the study as such solvents have been clearly shown in the scientific literature to compete with XB interactions.[40,53,78,79]

In our study, similar to Sarwar and co-workers' findings with polar solvents of chloroform and DMSO,[40] we observed solvents of high polarity[80] to significantly weaken XB interactions. For example, chloroform and dichloromethane

(DCM), two of the most polar solvents tested in this study, yielded nearly negligible K_a values of 0 and 0.6 M^{-1}, respectively (i.e., no XB interaction). Specifically, these two solvents engage in strong dipole−dipole interactions with Bu$_3$PO, introduce non-XB interactions, and thus decrease the extent of XB interactions between IPFB and Bu$_3$PO. In notable contrast to Sarwar et al.'s finding with DCM that showed minimal effect on XB strength,[40] DCM significantly interferes with XB interactions.

XB interactions of IPFB with Bu$_3$PO in aromatic hydrocarbon-based solvents (i.e., benzene, p-xylene, and toluene) resulted in very similar K_a values in the range of 5−8 M^{-1}. While these K_a values are significantly greater than those observed in more polar solvents, they are still lower than the K_a value seen in cyclohexane (22.08 M^{-1}). It is hypothesized that with aromatic solvents, XB remains a prominent component of the total intermolecular interactions, but there are competing intermolecular π−π interactions (i.e., π-stacking) between the IPFB and benzene, p-xylene, and toluene which affect the extent of XB interactions. Comparing the same system tested in cyclohexane *versus* benzene best illustrates the potential effects of this point. IPFB interacting with Bu$_3$PO or Oct$_3$PO in cyclohexane results in high K_a values of 44.02 and 22.08 M^{-1}, respectively. However, when the same systems are tested in benzene, the strength of XB interactions diminishes by 75% for Bu$_3$PO (K_a = 5.66 M^{-1}) and 67% for Oct$_3$PO (K_a = 14.24 M^{-1}) (Table 4). Bolstering this concept, Sarwar et al.'s results show a minimal drop in K_a value, 2.8 to 2.6 M^{-1}, when the same system is tested in cyclohexane *versus* benzene using the XB donor iodoperfluorooctane with no ability to engage in π-stacking.[40] Additionally, the literature reports suggest that lone pair-π interactions between the lone pair of the oxygen of XB acceptors and the π-cloud of IPFB and benzene may also compete with XB interactions.[53,81]

The results of Table 4 also indicate that solvent polarity is not the only solvent effect to be considered. For example, IPFB−Bu$_3$PO tested in diethyl ether and carbon tetrachloride, while having its K_a values decrease from that in cyclohexane, still exhibit substantial K_a values of 7.99 and 4.18 M^{-1}, respectively. In the case of diethyl ether, this is a higher K_a value than expected given that its dipole is similar to solvents that clearly diminished XB (i.e., chloroform and dichloromethane). For carbon tetrachloride with a net zero dipole, the K_a value is far lower than expected given the non-polar nature of the solvent. In this latter case, there is precedent in the literature for XB with CCl$_4$. Computational reports[82,83] and experimental evidence[46] have suggested that CCl$_4$ itself can function as an XB donor and thus interact with Bu$_3$PO as well. This secondary, competing interaction of CCl$_4$ solvent diminishes the primary XB interaction between IPFB and Bu$_3$PO, especially given its presence in far greater concentration as a solvent. That said, the measured K_a value is still believed to reflect the XB interaction between IPFB and Bu$_3$PO given that the corresponding binding isotherm plateaued with increasing concentration of Bu$_3$PO during titration (Supporting Information, Figure S62).

The IPFB−Bu$_3$PO system in diethyl ether represents an opportunity to illustrate the other types of effects, aside from polarity, that can affect XB interactions. As previously noted from the Taylor group's work[40] and the use of XB in separation science,[10,11] it is useful to examine established polarity indices/parameters to understand how collective solvent properties can impact XB interactions. One such

parameter is the Snyder polarity index, derived from solubility data of standard solutes in over 80 different solvents collected by Rohrschneider,[84] that classifies solvents based on three major properties (dipole/polarity, proton acceptor ability, and proton donor ability) that contribute to an overall Snyder polarity index.[85] The Snyder indices for the solvents used as part of this have been included in Table 4. The Snyder classification system helps explain why diethyl ether yields a significantly higher K_a for the test system compared to other solvents with similar dipole characteristics (chloroform and dichloromethane), see Table 4. While the dipoles of chloroform and dichloromethane are similar, the Snyder polarity indices differ largely because diethyl ether is a Lewis base solvent with a significantly larger proton acceptor (or lone-pair donor) property in comparison to the other solvents. A similar trend can be inferred if one applies Catalán's solvatochromic parameters which similarly characterize solvents with three parameters: solvent basicity (SB), solvent acidity (SA), and solvent polarizability (i.e., dipolarity).[80] Here again, the Catalán scale shows that chloroform and dichloromethane have comparable SA and SB parameters whereas diethyl ether exhibits negligible SA parameter and dominant SB character to arrive at similar overall solvent polarity. This type of behavior is also observed with other proton acceptor (or lone-pair donor; Lewis-base type) solvents (e.g., acetonitrile, tetrahydrofuran, and triethylamine). Using solvent indices of this nature allows the prediction of the effect of solvent on the relative XB interaction strength.

3.4. ^{19}F−^{1}H HOESY NMR Measurements of XB Interactions.

As previously discussed, K_a values reflect the strength of XB interaction within an adduct as a function of structural and electronic properties of both XB donor and acceptor. Within this study, the assumption is that the magnitude of the K_a values determined by the NMR titrations reflects the strength of specific XB interactions. 2D NMR techniques such as ^{1}H−^{1}H NOESY and ^{19}F−^{1}H HOESY have proven to be effective tools for assessing the specific nature and degree of intermolecular interactions as described in detail in a 2015 review by Ciancaleoni.[86] In a more specific study, Ciancaleoni and co-workers employed ^{19}F−^{1}H HOESY NMR and computational chemistry to explore solvent effects on XB interaction strength, finding that adducts of IPFB with Me$_3$Py (XB acceptor) exhibited decreasing XB/non-XB ratios of 94:6, 91:9, and 58:42 in cyclohexane, toluene, and methanol, respectively.[53] More recently, Otte et al. used ^{1}H−^{1}H NOESY NMR with a weak XB donor (iodobenzene) and a strong XB acceptor (quinuclidine) to show weak XB interactions in the presence of other non-XB interactions (i.e., nitrogen−π and π stacking).[52]

Herein, ^{19}F−^{1}H HOESY NMR is used to reinforce the K_a values determined from the NMR titrations and provide a greater understanding of the meaningfulness of their magnitude. In the case of XB adducts in this study, the ^{19}F−^{1}H HOESY NMR technique can provide critical evidence of specific cross-coupling between the *ortho* F atoms of the XB donor IPFB and specific protons of the XB acceptors. For this NMR technique, it is critical to first optimize the S/N ratio of the NMR measurements. This optimization was accomplished by performing repetitive ^{19}F−^{1}H HOESY NMR measurements of the IPFB−Oct$_3$PO system in cyclohexane (K_a = 44.02 ± 1.02 M^{-1}) and varying the NMR mixing time (d_8) between 400 and 1200 ms (Supporting Information, Figures S67−S70). The d_8 parameter proved to be consequential in affecting the
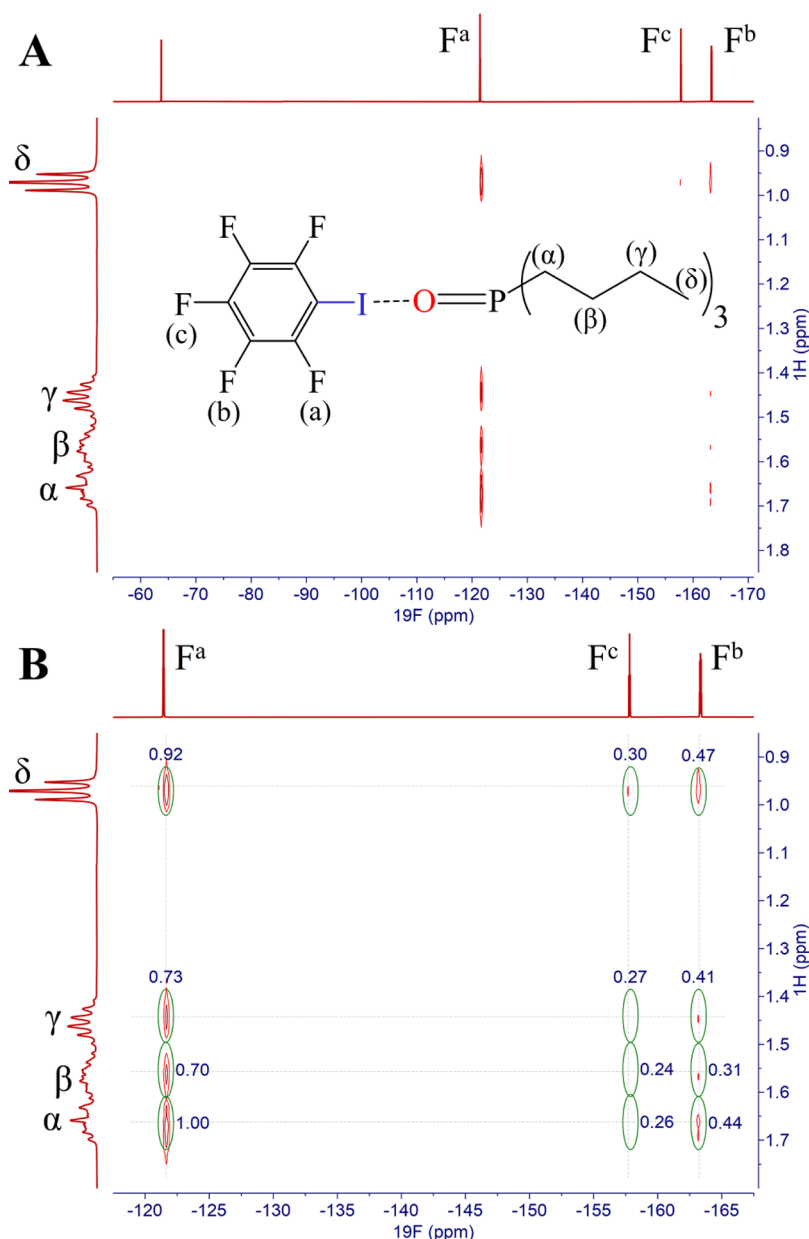
Figure 6. (A) ^{19}F−^{1}H HOESY NMR full spectrum of a mixture of IPFB (0.0525 M) with Bu$_3$PO (1.0 M) in cyclohexane and (B) expansion of the spectrum with assigned coupling interactions and cross-peak intensities. Note: ^{19}F−^{1}H HOESY spectra for other XB adducts (Table 5) can be found in Supporting Information (Figures S69, S72, and S73).

S/N ratio with a mixing time of 800 ms producing the highest S/N ratio (21:1)—see Supporting Information (Figure S71). An NMR mixing time (d_8) of 800 ms was thus applied to all subsequent ^{19}F−^{1}H HOESY NMR measurements on other systems where S/N ratios were found to range between 16:1 and 20:1.

Several specific systems were strategically selected for analysis with ^{19}F−^{1}H HOESY NMR in order to provide reference for NMR titration-measured K_a values and further understand the suspected structural impacts identified in the study. For each NMR experiment, the XB donor IPFB was saturated with a specific XB acceptor to ensure that >90% of IPFB is bound with the acceptor molecules, corresponding to the plateau of the binding isotherms during NMR titrations. Figure 6 displays a representative example of the ^{19}F−^{1}H HOESY NMR spectrum collected for the IPFB−Bu$_3$PO

adduct in cyclohexane (K_a = 22.08 M^{-1})—one of the stronger XB systems identified in our study. The spectrum and data for IPFB−Bu$_3$PO show that the strongest interactions are between the *ortho*-F^a and the H$^\alpha$ and H$^\delta$ protons followed by interactions with the H$^\beta$ and H$^\gamma$ protons of Bu$_3$PO (Figure 6B, Table 5). As expected for XB interaction at IPFB's σ-hole, interactions of Bu$_3$PO's protons with IPFB's F^b and F^c were substantially less. One could argue that the HOESY cross-peak intensities between the protons of the butyl groups and the fluorines of IPFB could result from other bimolecular interactions. However, the high correlation of H$^\alpha$ and *ortho*-F^a in the IPFB−Bu$_3$PO adduct strongly suggests that XB is the dominant interaction in the sample and that the correlation is a consequence of XB interaction, as opposed to originating from some other contrived combination of non-selective interactions that fortuitously bring H$^\alpha$ and *ortho*-F^a into proximity.

Table 5. ^{19}F–^{1}H HOESY Cross-Peak Relative Intensities from XB Adducts

XB Adduct of IPFB and Bu$_3$PO in d$_{12}$-Cyclohexane (K_a = 22.08 ± 1.02 M^{-1})

^{1}H	F^a	F^b	F^c
α	1.00	0.44	0.26
β	0.70	0.31	0.24
γ	0.73	0.41	0.27
δ	0.92	0.47	0.30

XB Adduct of IPFB and Oct$_3$PO in d$_{12}$-Cyclohexane (K_a = 44.02 ± 1.02 M^{-1})

^{1}H	F^a	F^b	F^c
1, 3	0.58	0.37	0.23
2	0.33	0.23	0.12
4, 5, 6, 7	1.00	0.76	0.37
8	0.18	0.18	0.10

XB Adduct of IPFB and Bu$_3$PO in d$_6$-Benzene (K_a = 5.66 ± 0.15 M^{-1})

^{1}H	F^a	F^b	F^c
α	1.00	0.89	0.43
β	0.41	0.33	0.25
γ	0.56	0.45	0.32
δ	0.72	0.54	0.27

XB Adduct of IPFB and Oct$_3$PO in d$_6$-Benzene (K_a = 14.24 ± 2.03 M^{-1})

^{1}H	F^a	F^b	F^c
1	0.35	0.20	0.11
2	0.51	0.27	0.15
3	0.33	0.23	0.11
4, 5, 6, 7	1.00	0.54	0.27
8	0.15	0.18	0.11

XB Adduct of IPFB and Bu$_3$PO in d-Chloroform (K_a = 0 M^{-1})

^{1}H	F^a	F^b	F^c
α			
β			
γ	S/N ratio was low. No cross-peaks were detected.		
δ			

XB Adduct of IPFB and Oct$_3$PO in d-chloroform (K_a = 0 M^{-1})

^{1}H	F^a	F^b	F^c
1			
2			
3	S/N ratio was low. No cross-peaks were detected.		
4, 5, 6, 7			
8			

^{19}F–^{1}H HOESY NMR spectra for the other systems tested are provided in Supporting Information (Figures S69, S72, and S73). Table 5 summarizes the specific interactions measured by ^{19}F–^{1}H HOESY NMR for each system tested by listing the relative intensities of the cross-coupled peaks. Overall, the HOESY spectra for IPFB–Bu$_3$PO reinforces the idea of the R groups playing a substantial role in stronger XB interactions (larger K_a values). Further evidence of this is derived from the spectrum (Supporting Information, Figure S69) and data (Table 5) collected for the IPFB–Oct$_3$PO system which was measured with the highest recorded K_a value (K_a = 44.02 M^{-1}) during NMR titrations. Here again, the most substantial cross-coupling occurs between protons at the end of the octyl group (H^{4,5,6,7}) and the *ortho* F of IPFB. These results suggest that the butyl and octyl groups of these XB acceptors are flexible enough to adopt conformations that stabilize the XB interaction as evident from the substantial ^{19}F–^{1}H cross-peaks.

NMR titrations revealed that the solvent could have a major impact on the strength of XB interactions, and additional ^{19}F–^{1}H HOESY NMR experiments were used to further explore this phenomenon. In addition to running the IPFB–

Bu$_3$PO and IPFB–Oct$_3$PO systems in cyclohexane as just described, they were also experimented in additional solvents of benzene and chloroform. A representative NMR titration result of IPFB–Oct$_3$PO adducts in chloroform is provided in Supporting Information (Figure S74), yielding a negligible K_a (0.0 M^{-1}). NMR titration of IPFB–Bu$_3$PO adducts in benzene revealed a nearly 4-fold drop in K_a compared to that in cyclohexane while IPFB–Bu$_3$PO adducts in chloroform exhibited a negligible K_a value (Table 4). Cross-couplings measured via ^{19}F–^{1}H HOESY NMR track with the K_a values where, despite the drop in K_a of IPFB–Bu$_3$PO in benzene, XB interactions remain strong enough to produce ^{19}F–^{1}H cross-peaks with high S/N ratio, though displaying significantly weaker cross-coupled peak intensities (Table 5 and Supporting Information, Figure S72). The weakening of the XB interaction in benzene may result from the introduction of non-XB interactions. While cross-peak integrals of H$^\beta$, H$^\gamma$, and H$^\delta$ with F^b and F^c are similar in cyclohexane and benzene, the cross-coupling interaction of H$^\alpha$ with F^b and F^c is higher in benzene than in cyclohexane, suggesting the possibility of competing lone pair–π system interactions. In chloroform, which yielded a negligible K_a via NMR titration, the corresponding cross-coupling peaks are completely absent (Table 5 and Supporting Information, Figure S73), reinforcing the concept that polar solvents can greatly hinder XB interactions. A similar pattern is observed for the IPFB–Oct$_3$PO system when results are compared across cyclohexane, benzene, and chloroform (Supporting Information, Figures S69, S72, and S73). Cross-peak integrals for ^{19}F–^{1}H interactions are non-existent in chloroform, whereas they are present and comparable for IPFB–Oct$_3$PO in both cyclohexane and benzene despite a 3-fold drop in K_a when the system is tested in benzene *versus* cyclohexane. Such a result suggests that the extent of non-XB interactions (e.g., lone pair–π system) does not increase significantly in benzene as seen with the IPFB–Bu$_3$PO system, which indicates that IPFB and Oct$_3$PO interact strongly via XB interaction. Overall, the ^{19}F–^{1}H HOESY NMR results appear to bolster several key findings regarding XB interactions: the stabilizing effect of alkyl chain R groups, the consequential effects of the solvent, and the affirmation that K_a values scale with physical interactions around the σ-hole of the XB donor structure.

4. CONCLUSIONS

In this study, NMR titrations, used in conjunction with DFT calculations, enabled the systematic testing and prediction of XB interaction strength as a function of both XB donor and acceptor molecular structure. The subsequent application of 2D NMR allowed us to correlate K_a values with specific physical interactions between protons on the XB acceptor and fluorine atoms on the XB donor. In general, the results suggest that K_a values ≥5 M^{-1} indicate significant XB interaction, whereas lower values suggest the presence of weak, non-specific interactions. The results of this study allow for several pertinent conclusions for understanding how the molecular structure impacts the strength of XB interactions. It is evident from both the computational modeling as well as the NMR titration data that the presence of *both* iodine and EWGs are required in the XB donor in order to induce strong XB interactions. The situation is somewhat more complex regarding the structure of the XB acceptor molecules which have three major components: the central atom, Lewis-base atom, and surrounding R groups. If all three of the components

are considered simultaneously, the overarching characteristic for strong XB interactions is the ability to direct e⁻ density toward the σ-hole. For the Lewis-base atom in direct contact with the XB donor's σ-hole, atoms of high EN (e.g., O vs S or Se) accomplish this while the central atom must simultaneously be low in EN and larger in atomic radii (P vs C or S) so as to not draw e⁻ density away from the XB interaction. Similarly, the presence of surrounding R groups allows for additional e⁻ density toward the central atom which, in turn, can help enhance the Lewis-base atom's e⁻-donating capability for stronger XB interactions.

A significant feature of our study, as confirmed by NMR titrations, DFT calculations, and 2D NMR measurements, is the previously unreported and surprising stabilizing effect of the XB acceptor's surrounding R groups. High K_a and low ΔE_{int} values, consistent with the intensity of ¹⁹F−¹H HOESY NMR cross-coupling peaks, were observed in specific systems involving longer chain R groups (butyl and octyl) on the XB acceptor. While the exact nature of this stabilization is not completely understood, results suggest that the longer chains are flexible enough to bend toward the XB donor, perhaps allowing for greater van der Waals interaction with the XB donor and/or providing a more hydrophobic XB acceptor front that effectively isolates and directs the Lewis-base atom's e⁻ density toward the σ-hole. Interestingly, when amine-based XB acceptors were examined, with nitrogen serving simultaneously as the central and Lewis-base atom, the same R group stabilization trend is observed for primary and secondary amines, albeit to a much lesser extent. These results suggest that the stabilizing effect of R groups is much more effective if the Lewis-base atom is separated from the central atom. Moreover, quinuclidine, a tertiary amine with rigid R groups, exhibited the most negative ΔE_{int} and highest K_a values of any amine-based XB acceptor. Such results suggest that when amine-based XB acceptors are involved, XB benefits from the R groups being more rigid are less likely to flex toward the XB donor. A final conclusion of the study is that experimental NMR titrations of a system in various solvents clearly established that even when employing the most conducive molecular structure for strong XB in $solution$, the interaction remains heavily dependent on the nature of the solvent: non-polar, non-aromatic solvents promote stronger XB in solution. With a greater fundamental understanding of how the molecular structure of both the XB donor and acceptor molecules impact the strength of the XB interaction, this study provides a fundamental tool to better evaluate or predict XB interactions in solution.

ASSOCIATED CONTENT

Ⓢ Supporting Information

The Supporting Information is available free of charge at https://pubs.acs.org/doi/10.1021/acs.jpca.1c07554.

> Benchmarking and XB computational results, details of non-linear regression analysis method and program for analyzing binding isotherms, two-dimensional NMR measurements/spectra, optimized geometries of all XB adducts, initial ¹⁹F and ¹H spectra of all XB donors, and binding isotherms (or titration curves) from NMR titration experiments (PDF)

AUTHOR INFORMATION

Corresponding Author

Michael C. Leopold − $Department$ of $Chemistry,$ $Gottwald$ $Center$ for the $Sciences,$ $University$ of $Richmond,$ $Richmond,$ $Virginia$ $23173,$ $United$ $States;$ ⓞ orcid.org/0000-0001-6525-9281; Phone: +1-(804)-287-6329; Email: mleopold@richmond.edu

Authors

Quang Minh Dang − $Department$ of $Chemistry,$ $Gottwald$ $Center$ for the $Sciences,$ $University$ of $Richmond,$ $Richmond,$ $Virginia$ $23173,$ $United$ $States$

Jeffrey H. Simpson − $Department$ of $Chemistry,$ $Gottwald$ $Center$ for the $Sciences,$ $University$ of $Richmond,$ $Richmond,$ $Virginia$ $23173,$ $United$ $States$

Carol A. Parish − $Department$ of $Chemistry,$ $Gottwald$ $Center$ for the $Sciences,$ $University$ of $Richmond,$ $Richmond,$ $Virginia$ $23173,$ $United$ $States;$ ⓞ orcid.org/0000-0003-2878-3070

Complete contact information is available at:
https://pubs.acs.org/10.1021/acs.jpca.1c07554

ADDITIONAL NOTES

[a]NOTE: Use extreme caution when using benzene as it is a potential carcinogen; benzene was handled with proper personal protective equipment in small volume for each sample (≤1.00 mL) in this study.
[b]NOTE: Use extreme caution when using tributylamine (Bu₃N) as it can be particularly dangerous if the skin is exposed.

REFERENCES

(1) Cavallo, G.; Metrangolo, P.; Milani, R.; Pilati, T.; Priimagi, A.; Resnati, G.; Terraneo, G. The Halogen Bond. $Chem.$ $Rev.$ **2016**, 116, 2478−2601.

(2) Erdélyi, M. Halogen Bonding in Solution. *Chem. Soc. Rev.* **2012**, *41*, 3547−3557.

(3) Costa, P. J. The Halogen Bond: Nature and Applications. *Phys. Sci. Rev.* **2017**, *2*, 16.

(4) Mínguez Espallargas, G.; Zordan, F.; Arroyo Marín, L.; Adams, H.; Shankland, K.; van de Streek, J.; Brammer, L. Rational Modification of the Hierarchy of Intermolecular Interactions in Molecular Crystal Structures by Using Tunable Halogen Bonds. *Chem.—Eur. J.* **2009**, *15*, 7554−7568.

(5) Fourmigué, M. Halogen Bonding: Recent Advances. *Curr. Opin. Solid State Mater. Sci.* **2009**, *13*, 36−45.

(6) Metrangolo, P.; Resnati, G. CHEMISTRY: Halogen Versus Hydrogen. *Science* **2008**, *321*, 918−919.

(7) Berger, G.; Frangville, P.; Meyer, F. Halogen Bonding for Molecular Recognition: New Developments in Materials and Biological Sciences. *Chem. Commun.* **2020**, *56*, 4970−4981.

(8) Parker, A. J.; Stewart, J.; Donald, K. J.; Parish, C. A. Halogen Bonding in DNA Base Pairs. *J. Am. Chem. Soc.* **2012**, *134*, 5165−5172.

(9) Lu, Y.; Shi, T.; Wang, Y.; Yang, H.; Yan, X.; Luo, X.; Jiang, H.; Zhu, W. Halogen Bonding-a Novel Interaction for Rational Drug Design? *J. Med. Chem.* **2009**, *52*, 2854−2862.

(10) Dallocchio, R.; Dessì, A.; Solinas, M.; Arras, A.; Cossu, S.; Aubert, E.; Mamane, V.; Peluso, P. Halogen Bond in High-Performance Liquid Chromatography Enantioseparations: Description, Features and Modelling. *J. Chromatogr. A* **2018**, *1563*, 71−81.

(11) Peluso, P.; Mamane, V.; Dessì, A.; Dallocchio, R.; Aubert, E.; Gatti, C.; Mangelings, D.; Cossu, S. Halogen Bond in Separation Science: A Critical Analysis across Experimental and Theoretical Results. *J. Chromatogr. A* **2020**, *1616*, 460788.

(12) Langton, M. J.; Robinson, S. W.; Marques, I.; Félix, V.; Beer, P. D. Halogen Bonding in Water Results in Enhanced Anion Recognition in Acyclic and Rotaxane Hosts. *Nat. Chem.* **2014**, *6*, 1039−1043.

(13) Lim, J. Y. C.; Marques, I.; Ferreira, L.; Félix, V.; Beer, P. D. Enhancing the Enantioselective Recognition and Sensing of Chiral Anions by Halogen Bonding. *Chem. Commun.* **2016**, *52*, 5527−5530.

(14) Weis, J. G.; Ravnsbæk, J. B.; Mirica, K. A.; Swager, T. M. Employing Halogen Bonding Interactions in Chemiresistive Gas Sensors. *ACS Sens.* **2016**, *1*, 115−119.

(15) Mullaney, B. R.; Cunningham, M. J.; Davis, J. J.; Beer, P. D. Acyclic Halogen and Hydrogen Bonding Diquat-Containing Receptors for the Electrochemical Sensing of Anions. *Polyhedron* **2016**, *116*, 20−25.

(16) Gale, P. A.; Caltagirone, C. Fluorescent and Colorimetric Sensors for Anionic Species. *Coord. Chem. Rev.* **2018**, *354*, 2−27.

(17) Jaini, A. K. A.; Hughes, L. B.; Kitimet, M. M.; Ulep, K. J.; Leopold, M. C.; Parish, C. A. Halogen Bonding Interactions for Aromatic and Nonaromatic Explosive Detection. *ACS Sens.* **2019**, *4*, 389−397.

(18) Desiraju, G. R.; Ho, P. S.; Kloo, L.; Legon, A. C.; Marquardt, R.; Metrangolo, P.; Politzer, P.; Resnati, G.; Rissanen, K. Definition of the Halogen Bond (Iupac Recommendations 2013). *Pure Appl. Chem.* **2013**, *85*, 1711−1713.

(19) Politzer, P.; Murray, J. S.; Clark, T. Halogen Bonding: An Electrostatically-Driven Highly Directional Noncovalent Interaction. *Phys. Chem. Chem. Phys.* **2010**, *12*, 7748−7757.

(20) Clark, T.; Hennemann, M.; Murray, J. S.; Politzer, P. Halogen bonding: the σ-hole. *J. Mol. Model.* **2007**, *13*, 291−296.

(21) Borissov, A.; Marques, I.; Lim, J. Y. C.; Félix, V.; Smith, M. D.; Beer, P. D. Anion Recognition in Water by Charge-Neutral Halogen and Chalcogen Bonding Foldamer Receptors. *J. Am. Chem. Soc.* **2019**, *141*, 4119−4129.

(22) Mullaney, B. R.; Thompson, A. L.; Beer, P. D. An All-Halogen Bonding Rotaxane for Selective Sensing of Halides in Aqueous Media. *Angew. Chem. Int. Ed.* **2014**, *53*, 11458−11462.

(23) Voth, A. R.; Hays, F. A.; Ho, P. S. Directing Macromolecular Conformation through Halogen Bonds. *Proc. Natl. Acad. Sci. U.S.A.* **2007**, *104*, 6188−6193.

(24) Sun, A.; Lauher, J. W.; Goroff, N. S. Preparation of Poly(Diiododiacetylene), an Ordered Conjugated Polymer of Carbon and Iodine. *Science* **2006**, *312*, 1030−1034.

(25) Corradi, E.; Meille, S. V.; Messina, M. T.; Metrangolo, P.; Resnati, G. Halogen Bonding Versus Hydrogen Bonding in Driving Self-Assembly Processes. *Angew. Chem., Int. Ed.* **2000**, *39*, 1782−1786.

(26) Corradi, E.; Meille, S. V.; Messina, M. T.; Metrangolo, P.; Resnati, G. Perfluorocarbon-Hydrocarbon Self-Assembly, Part Ix. Halogen Bonding Versus Hydrogen Bonding in Driving Self-Assembly Processes. *Angew. Chem. Int. Ed.* **2000**, *39*, 1782.

(27) Robertson, C. C.; Wright, J. S.; Carrington, E. J.; Perutz, R. N.; Hunter, C. A.; Brammer, L. Hydrogen Bonding Vs. Halogen Bonding: The Solvent Decides. *Chem. Sci.* **2017**, *8*, 5392−5398.

(28) Shirman, T.; Kaminker, R.; Freeman, D.; van der Boom, M. E. Halogen-Bonding Mediated Stepwise Assembly of Gold Nanoparticles onto Planar Surfaces. *ACS Nano* **2011**, *5*, 6553−6563.

(29) Zamborini, F. P.; Leopold, M. C.; Hicks, J. F.; Kulesza, P. J.; Malik, M. A.; Murray, R. W. Electron Hopping Conductivity and Vapor Sensing Properties of Flexible Network Polymer Films of Metal Nanoparticles. *J. Am. Chem. Soc.* **2002**, *124*, 8958−8964.

(30) Tognarelli, D. J.; Miller, R. B.; Pompano, R. R.; Loftus, A. F.; Sheibley, D. J.; Leopold, M. C. Covalently Networked Monolayer-Protected Nanoparticle Films. *Langmuir* **2005**, *21*, 11119−11127.

(31) Ai, K.; Liu, Y.; Lu, L. Hydrogen-Bonding Recognition-Induced Color Change of Gold Nanoparticles for Visual Detection of Melamine in Raw Milk and Infant Formula. *J. Am. Chem. Soc.* **2009**, *131*, 9496−9497.

(32) Tawfik, M.; Donald, K. J. Halogen Bonding: Unifying Perspectives on Organic and Inorganic Cases. *J. Phys. Chem. A* **2014**, *118*, 10090−10100.

(33) Donald, K. J.; Tawfik, M. The Weak Helps the Strong: Sigma-Holes and the Stability of MF4·Base Complexes. *J. Phys. Chem. A* **2013**, *117*, 14176−14183.

(34) Donald, K. J.; Wittmaack, B. K.; Crigger, C. Tuning σ-Holes: Charge Redistribution in the Heavy (Group 14) Analogues of Simple and Mixed Halomethanes Can Impose Strong Propensities for Halogen Bonding. *J. Phys. Chem. A* **2010**, *114*, 7213−7222.

(35) Lu, Y.-X.; Zou, J.-W.; Wang, Y.-H.; Jiang, Y.-J.; Yu, Q.-S. Ab Initio Investigation of the Complexes between Bromobenzene and Several Electron Donors: Some Insights into the Magnitude and Nature of Halogen Bonding Interactions. *J. Phys. Chem. A* **2007**, *111*, 10781−10788.

(36) Ford, M. C.; Saxton, M.; Ho, P. S. Sulfur as an Acceptor to Bromine in Biomolecular Halogen Bonds. *J. Phys. Chem. Lett.* **2017**, *8*, 4246−4252.

(37) Shirman, T.; Boterashvili, M.; Orbach, M.; Freeman, D.; Shimon, L. J. W.; Lahav, M.; van der Boom, M. E. Finding the Perfect Match: Halogen Vs Hydrogen Bonding. *Cryst. Growth Des.* **2015**, *15*, 4756−4759.

(38) Li, Q.-Z.; Jing, B.; Li, R.; Liu, Z.-B.; Li, W.-Z.; Luan, F.; Cheng, J.-B.; Gong, B.-A.; Sun, J.-Z. Some Measures for Making Halogen Bonds Stronger Than Hydrogen Bonds in H2cs-Hox (X = F, Cl, and Br) Complexes. *Phys. Chem. Chem. Phys.* **2011**, *13*, 2266−2271.

(39) Aakeröy, C. B.; Fasulo, M.; Schultheiss, N.; Desper, J.; Moore, C. Structural Competition between Hydrogen Bonds and Halogen Bonds. *J. Am. Chem. Soc.* **2007**, *129*, 13772.

(40) Sarwar, M. G.; Dragisic, B.; Salsberg, L. J.; Gouliaras, C.; Taylor, M. S. Thermodynamics of Halogen Bonding in Solution: Substituent, Structural, and Solvent Effects. *J. Am. Chem. Soc.* **2010**, *132*, 1646−1653.

(41) Joksch, M.; Agarwala, H.; Ferro, M.; Michalik, D.; Spannenberg, A.; Beweries, T. A Comparative Study on the Thermodynamics of Halogen Bonding of Group 10 Pincer Fluoride Complexes. *Chem.—Eur. J.* **2020**, *26*, 3571−3577.

(42) Guo, N.; Maurice, R.; Teze, D.; Graton, J.; Champion, J.; Montavon, G.; Galland, N. Experimental and Computational Evidence of Halogen Bonds Involving Astatine. *Nat. Chem.* **2018**, *10*, 428−434.

(43) Hauchecorne, D.; Moiana, A.; van der Veken, B. J.; Herrebout, W. A. Halogen Bonding to a Divalent Sulfur Atom: An Experimental Study of the Interactions of Cf3x (X = Cl, Br, I) with Dimethyl Sulfide. *Phys. Chem. Chem. Phys.* **2011**, *13*, 10204−10213.

(44) Hettstedt, C.; Mayer, P.; Karaghiosoff, K. Halogen Bonding in the Crystal Structures of 1,2-Diiodo Alkenes. *New J. Chem.* **2015**, *39*, 8522−8533.

(45) Nguyen, H. L.; Horton, P. N.; Hursthouse, M. B.; Legon, A. C.; Bruce, D. W. Halogen Bonding: A New Interaction for Liquid Crystal Formation. *J. Am. Chem. Soc.* **2004**, *126*, 16−17.

(46) Rosokha, S. V.; Neretin, I. S.; Rosokha, T. Y.; Hecht, J.; Kochi, J. K. Charge-transfer character of halogen bonding: Molecular structures and electronic spectroscopy of carbon tetrabromide and bromoform complexes with organic σ- and π-donors. *Heteroat. Chem.* **2006**, *17*, 449−459.

(47) Hawthorne, B.; Fan-Hagenstein, E.; Smith, J.; Hanks, T. Study of the Halogen Bonding between Pyridine and Perfluoroalkyl Iodide in Solution Phase Using the Combination of FTIR and ¹⁹F NMR. *Int. J. Spectrosc.* **2013**, *2013*, 1−10.

(48) Shen, Q. J.; Jin, W. J. Strong Halogen Bonding of 1,2-Diiodoperfluoroethane and 1,6-Diiodoperfluorohexane with Halide Anions Revealed by Uv-Vis, Ft-Ir, Nmr Spectroscopes and Crystallography. *Phys. Chem. Chem. Phys.* **2011**, *13*, 13721−13729.

(49) Schulz, N.; Schindler, S.; Huber, S. M.; Erdelyi, M. Nmr Determination of the Binding Constant of Ionic Species: A Caveat. *J. Org. Chem.* **2018**, *83*, 10881−10886.

(50) Thordarson, P. Determining Association Constants from Titration Experiments in Supramolecular Chemistry (Vol 40, Pg 1305, 2011). *Chem. Soc. Rev.* **2011**, *40*, 1305.

(51) Maugeri, L.; Asencio-Hernández, J.; Lébl, T.; Cordes, D. B.; Slawin, A. M. Z.; Delsuc, M.-A.; Philp, D. Neutral Iodotriazoles as Scaffolds for Stable Halogen-Bonded Assemblies in Solution. *Chem. Sci.* **2016**, *7*, 6422−6428.

(52) Otte, F.; Kleinheider, J.; Hiller, W.; Wang, R.; Englert, U.; Strohmann, C. Weak yet Decisive: Molecular Halogen Bond and Competing Weak Interactions of Iodobenzene and Quinuclidine. *J. Am. Chem. Soc.* **2021**, *143*, 4133−4137.

(53) Ciancaleoni, G.; Bertani, R.; Rocchigiani, L.; Sgarbossa, P.; Zuccaccia, C.; Macchioni, A. Discriminating Halogen-Bonding from Other Noncovalent Interactions by a Combined Noe Nmr/Dft Approach. *Chem.—Eur. J.* **2015**, *21*, 440−447.

(54) Cabot, R.; Hunter, C. A. Non-Covalent Interactions between Iodo-Perfluorocarbons and Hydrogen Bond Acceptors. *Chem. Commun.* **2009**, 2005−2007.

(55) Kolář, M. H.; Hobza, P. Computer Modeling of Halogen Bonds and Other Sigma-Hole Interactions. *Chem. Rev.* **2016**, *116*, 5155−5187.

(56) Kozuch, S.; Martin, J. M. L. Halogen Bonds: Benchmarks and Theoretical Analysis. *J. Chem. Theory Comput.* **2013**, *9*, 1918−1931.

(57) Siiskonen, A.; Priimagi, A. Benchmarking Dft Methods with Small Basis Sets for the Calculation of Halogen-Bond Strengths. *J. Mol. Model.* **2017**, *23*, 50.

(58) Zhu, Z.; Xu, Z.; Zhu, W. Interaction Nature and Computational Methods for Halogen Bonding: A Perspective. *J. Chem. Inf. Model.* **2020**, *60*, 2683−2696.

(59) Bartlett, R. J.; Musiał, M. Coupled-Cluster Theory in Quantum Chemistry. *Rev. Mod. Phys.* **2007**, *79*, 291−352.

(60) Frisch, M. J.; Trucks, G. W.; Schlegel, H. B.; Scuseria, G. E.; Robb, M. A.; Cheeseman, J. R.; Scalmani, G.; Barone, V.; Petersson, G. A.; Nakatsuji, H. *Gaussian 16*; Gaussian Inc.: Wallington, CT, 2016.

(61) Zhao, Y.; Truhlar, D. G. The M06 Suite of Density Functionals for Main Group Thermochemistry, Thermochemical Kinetics, Noncovalent Interactions, Excited States, and Transition Elements: Two New Functionals and Systematic Testing of Four M06-Class Functionals and 12 Other Functionals. *Theor. Chem. Acc.* **2008**, *120*, 215−241.

(62) Dunning, T. H. Gaussian basis sets for use in correlated molecular calculations. I. The atoms boron through neon and hydrogen. *J. Chem. Phys.* **1989**, *90*, 1007−1023.

(63) Kendall, R. A.; Dunning, T. H.; Harrison, R. J. Electron affinities of the first-row atoms revisited. Systematic basis sets and wave functions. *J. Chem. Phys.* **1992**, *96*, 6796−6806.

(64) Peterson, K. A.; Shepler, B. C.; Figgen, D.; Stoll, H. On the Spectroscopic and Thermochemical Properties of Clo, Bro, Io, and Their Anions. *J. Phys. Chem. A* **2006**, *110*, 13877−13883.

(65) Stoll, H.; Metz, B.; Dolg, M. Relativistic energy-consistent pseudopotentials?Recent developments. *J. Comput. Chem.* **2002**, *23*, 767−778.

(66) Tomasi, J.; Mennucci, B.; Cammi, R. Quantum Mechanical Continuum Solvation Models. *Chem. Rev.* **2005**, *105*, 2999−3094.

(67) Dennington, R.; Keith, T. A.; Millam, J. M. *Gaussview*; Semichem Inc.: Shawnee Mission, KS, 2016.

(68) Simpson, J. H. *Nmr Case Studies—Data Analysis of Complicated Molecules*; Elsevier, 2017; p 234.

(69) Libri, S.; Jasim, N. A.; Perutz, R. N.; Brammer, L. Metal Fluorides Form Strong Hydrogen Bonds and Halogen Bonds: Measuring Interaction Enthalpies and Entropies in Solution. *J. Am. Chem. Soc.* **2008**, *130*, 7842.

(70) Hughes, M. P.; Smith, B. D. Enhanced Carboxylate Binding Using Urea and Amide-Based Receptors with Internal Lewis Acid Coordination: A Cooperative Polarization Effect. *J. Org. Chem.* **1997**, *62*, 4492−4499.

(71) Venkitakrishnan, R. P.; Benard, O.; Max, M.; Markley, J. L.; Assadi-Porter, F. M. Use of Nmr Saturation Transfer Difference Spectroscopy to Study Ligand Binding to Membrane Proteins. In *Membrane Protein Structure and Dynamics: Methods and Protocols*; Vaidehi, N., Klein-Seetharaman, J., Ed.; Humana Press: Totowa, NJ, 2012; pp 47−63.

(72) Yu, J.-X.; Hallac, R. R.; Chiguru, S.; Mason, R. P. New frontiers and developing applications in 19F NMR. *Prog. Nucl. Magn. Reson. Spectrosc.* **2013**, *70*, 25−49.

(73) Schwerdtfeger, P.; Nagle, J. K. 2018 Table of static dipole polarizabilities of the neutral elements in the periodic table. *Mol. Phys.* **2019**, *117*, 1200−1225.

(74) Arman, H. D.; Rafferty, E. R.; Bayse, C. A.; Pennington, W. T. Complementary Selenium···Iodine Halogen Bonding and Phenyl Embraces: Cocrystals of Triphenylphosphine Selenide with Organo-iodides. *Cryst. Growth Des.* **2012**, *12*, 4315−4323.

(75) Chernysheva, M. V.; Rautiainen, J. M.; Ding, X.; Haukka, M. The Se Center Dot Center Dot Center Dot Hal Halogen Bonding: Co-Crystals of Selenoureas with Fluorinated Organohalides. *J. Solid State Chem.* **2021**, *295*, 121930.

(76) Metrangolo, P.; Panzeri, W.; Recupero, F.; Resnati, G. Perfluorocarbon-Hydrocarbon Self-Assembly - Part 16. F-19 Nmr Study of the Halogen Bonding between Halo-Perfluorocarbons and Heteroatom Containing Hydrocarbons. *J. Fluorine Chem.* **2002**, *114*, 27−33.

(77) Messina, M. T.; Metrangolo, P.; Panzeri, W.; Ragg, E.; Resnati, G. Perfluorocarbon-Hydrocarbon Self-Assembly. Part 3. Liquid Phase Interactions between Perfluoroalkylhalides and Heteroatom Containing Hydrocarbons. *Tetrahedron Lett.* **1998**, *39*, 9069−9072.

(78) Robertson, C. C.; Perutz, R. N.; Brammer, L.; Hunter, C. A. A Solvent-Resistant Halogen Bond. *Chem. Sci.* **2014**, *5*, 4179−4183.

(79) Wang, H.; Shen, Q. J.; Wang, W. Weakening and Leveling Effect of Solvent Polarity on Halogen Bond Strength of Diiodoper-fluoroalkane with Halide. *J. Solution Chem.* **2017**, *46*, 1092−1103.

(80) Reichardt, C. W. *Thomas, Solvents and Solvent Effects in Organic Chemistry*; Wiley-VCH Germany, 2010.

(81) Gamez, P.; Mooibroek, T. J.; Teat, S. J.; Reedijk, J. Anion Binding Involving π-Acidic Heteroaromatic Rings. *Acc. Chem. Res.* **2007**, *40*, 435−444.

(82) Mu, X.; Wang, Q.; Wang, L.-P.; Fried, S. D.; Piquemal, J.-P.; Dalby, K. N.; Ren, P. Modeling Organochlorine Compounds and the σ-Hole Effect Using a Polarizable Multipole Force Field. *J. Phys. Chem. B* **2014**, *118*, 6456−6465.

(83) Wang, P.; Zhao, N.; Tang, Y. Halogen Bonding in the Complexes of Ch3i and Ccl4 with Oxygen-Containing Halogen-Bond Acceptors. *J. Phys. Chem. A* **2017**, *121*, 5045−5055.

(84) Rohrschneider, L. Solvent Characterization by Gas-Liquid Partition Coefficients of Selected Solutes. *Anal. Chem.* **1973**, *45*, 1241−1247.

(85) Snyder, L. R. Classification of the Solvent Properties of Common Liquids. *J. Chromatogr.* **1974**, *92*, 223−230.

(86) Ciancaleoni, G. Characterization of Halogen Bonded Adducts in Solution by Advanced Nmr Techniques. *Magnetochemistry* **2017**, *3*, 30.